Problems of Planetology, Cosmochemistry and Meteoritica

Barenbaum A.A.[1], Shpekin M.I.[2] On question of origin and age of orientale basin on Moon.

UDC: 523.34-834

[1]*Oil and Gas Research Institute RAS, Moscow* (azary@mail.ru), [2]*Kazan Federal University, Kazan* (michaels1@yandex.ru)

Abstract. The Oriental Basin is considered to be the youngest multi-ring basin on the Moon. The basin age, however, is unknown and its determination is a very difficult problem. The outer diameter of Oriental Basin is 930 km, the basin itself is located in the southern hemisphere of Moon on the eastern edge of the vast highlands surrounding from the north the giant South Pole–Aitken (SPA) Basin with a diameter of 3000 km, the largest in Solar System. Previously, we put forward a hypothesis that the SPA Basin and the highlands adjacent to it from the north were formed in the Cenozoic (last 65 million years) as a result of 4 bombardments by galactic comets that falling in the southern hemisphere of Moon at small angles to its rotation axis. In this article in developing this hypothesis, we concluded that the Orientale Basin was formed about ~1 Ma during the last bombardment of Moon by galactic comets of the Orion-Cygnus jet stream. To substantiate this conclusion, we used measurements of comet flux density in this jet stream, invoked a new explanation of the giant South Pole–Aitken Basin origin by galactic comets, as well as analyzed the distribution density of large craters in floor of Orientale Basin.

Keywords: Orientale and South Pole-Aitken basins on Moon, galactic comets of Orion-Cygnus jet stream.

Introduction The Orientale Basin is considered the youngest multi-ring basin on the Moon. Although its age has not yet been established, as well as itself origin of this basin is debatable. The center of the Orientale Basin has coordinates: 19°54′S. and 94°42′ E, and it is located in the southern hemisphere of the Moon on the eastern edge of the vast highlands surrounding from the north the largest South Pole–Aitken (SPA) Basin in the Solar System with a diameter of 3000 km.

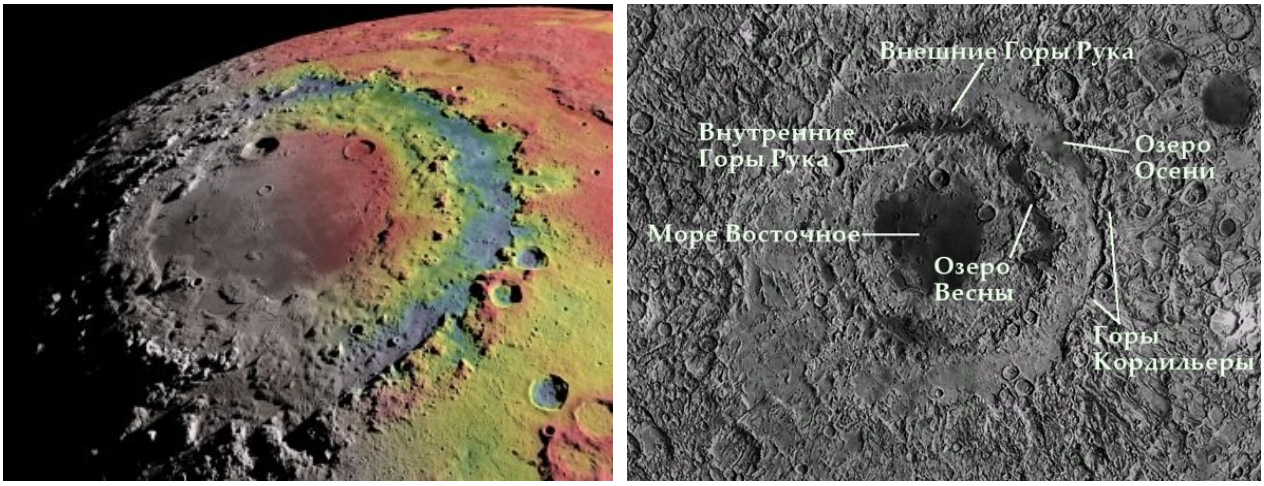

Fig. 1. Orientale Basin on the Moon: a) general view of the basin and b) its multi-ring structure

In the structure of the Orientale Basin (Fig. 1), three non-aligned rings can be distinguished, each of which is located at its own height level and is filled with lavas: one outer one – the Cordillera Mountains – with a diameter of 930 km, and two inner ones – the Rook's Mountains – with diameters of 160 and 430 km. The central part of the basin – the Eastern Sea, has an average altitude of –4.0 km. The layer of lavas in the East Sea reaches ≈ 1 km, which is less than in other seas on the visible side of the Moon. The areas between the outer and inner rings of the Rook's Mountains are at elevations from –2.0 to –2.5 km, and between the Rook's and Cordillera Mountains at elevations from –1.0 to 0.0 km.

In the northern part of the East Sea is a very young crater Maunder. On Fig. 2 shows the height profile of the central part of the Orientale Basin, passing from south to north through the Maunder Crater, according to the data of the Indian satellite Chandrayaan-1. Maunder crater in fig. 2 is located at a latitude of 15°S. The depth of the crater relative to the average surface of the Moon is –4.2 km.

Hypotheses of Orientale Basin origin There is a well-known hypothesis (Zuber et al., 2016), according to which the Orientale Basin arose 3.8 Ga, when the Moon was subjected to intense impacts of large asteroid bodies. Modeling showed that the asteroid that created this pool could have had a diameter of ≈64 km and fell at a speed of ≈14 km/s. The volume of rocks ejected in this case was estimated at least $(3.4\pm0.2)\times10^6$ km^3 (Johnson et al., 2016).

Previously (Barenbaum & Shpekin, 2020; Barenbaum & Shpekin, 2020a), we concluded that

the SPA basin and the highlands bordering it from the north, where the Orientale Basin is located, arose in the Cenozoic (the last 65 Ma) as a result of 4 bombardments by galactic comets falling into the southern hemisphere of the Moon at small angles to the axis of its rotation.

In the development of this hypothesis, in (Barenbaum & Shpekin, 2021), we believe that the Orientale Basin could have been formed by galactic comets that fell on the Moon at the end of their last bombardment, which occurred in the period from 5 to 0.7 Ma ago (Barenbaum, 2010). Therefore, the age of this basin is ~1 Ma, and the Maunder crater must be even younger.

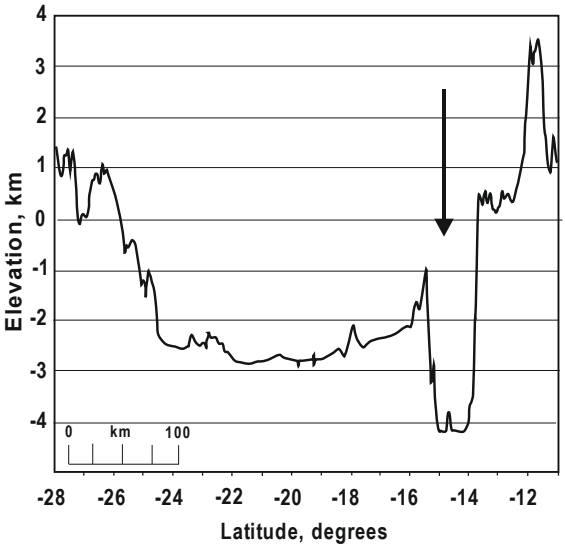

Fig. 2. Altitude profile of Orientale Basin passing through the center of the Maunder crater (shown by an arrow) according to the measurements of the Chandrayaan-1 satellite (Head et al., 2009)

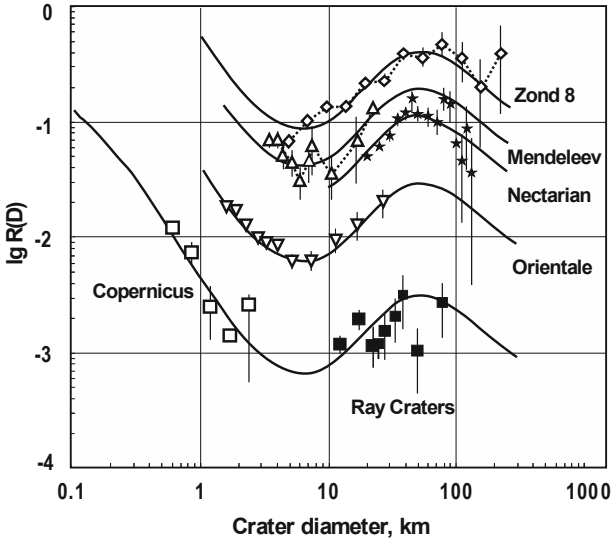

Fig. 3. Distribution of the density of craters in the seas of the Moon, as well as on the continents according to measurements by the automatic station Zond-8 (Neikum et al., 2001)

Substantiation of our comet hypothesis The works (Barenbaum, 2015; Barenbaum & Shpekin, 2016, 2018, 2018a, 2019, 2019a, 2019b, 2019c) show that huge craters and sea basins on the Moon, as well as on Mars and Mercury, were not formed as a result of large asteroid impacts (Melosh et al. 2013), but were created by bombardments of high-speed comets of galactic origin. These bombardments have the character of very intense cometary showers lasting 1–5 million years, which recurring every 20–37 million years during periods when the Sun is in the jet streams and spiral arms of the Galaxy (Barenbaum, 2010). At the same time, after ≈150–200 million years, galactic comets alternately bombard or the southern and northern hemispheres of the planets.

As a result, most craters 10–180 km in diameter and basins larger than 180 km on the Moon, Mars and Mercury were formed during the last bombardment and, to a lesser extent, during two or three previous comet bombardments, when comets mainly fell into the southern hemisphere of the planets (Barenbaum & Shpekin, 2011, 2016). The last cometary bombardment hit when the Solar System was in the Orion Cygnus jet stream of galactic comets, closest to the Sun. The last comet bombardment occurred when the Solar System was in the Orion Cygnus jet stream of galactic comets closest to the Sun. According to our estimates (Barenbaum, 2019; Barenbaum & Shpekin, 2021), a comet flux density was $\Phi \approx 5\times10^{-10}$ (year km^2)$^{-1}$. As a result, over the period of this bombardment $\Delta T \approx 4.3$ million years, the fallings density of these comets on the Earth and on other planets was $\approx 2 \times 10^{-3}$ km^{-2}. Thus, ≈150 comets should have fallen on an area of 100× 100 km^2 in the southern polar zone of the Moon.

At such a high comets falling density, the formed comet craters overlap each other, which leads to an increase in the diameter of the resulted emerging impact structure. We called this method of creating large craters and sea basins by galactic comets on the Moon "cumulative" (Barenbaum & Shpekin, 2018a). We explained the origin of the SPA basin with this mechanism (Barenbaum & Shpekin, 2020, 2020a), and in this paper we use it to estimate the age of the Orientale Basin (Barenbaum & Shpekin, 2021a).

Here are our arguments:

1) The Orientale Basin is located in the ejection zone of rocks from the SPA Basin, which, according to our data, was finally formed as a result of the last cometary bombardment in the period from 5.0 to 0.7

Ma. Consequently, the age of the Orientale Basin cannot exceed 5 million years.

2) With the Orientale Basin diameter of D = 930 km, during period of this bombardment $\Delta T \approx 4.3$ million years, $\approx 1.4 \times 10^3$ comets fell within its area, the energy of which is more than enough to create this basin (Barenbaum & Shpekin, 2019).

3) The Orientale Basin, however, could have arisen both at the beginning of the last bombardment and at its end. To clarify this time, consider the density of comet craters in it.

4) To refine this time, let us consider the density of comet craters at the Orientale Basin bottom (Fig. 3).

Figure 3 shows the distribution of craters in a number of marine basins, as well as those on the continents according measurement by the automatic station Zond-8 (Neukum et al., 2001). Cometary craters in Fig. 3 occupy the region D > 7 km. The density of such craters in all marine basins is lower than on the continents, at that in the Orientale Basin this difference is ~15 times. If we assume that during the bombardment period the frequency of galactic comet fallings on the Moon was constant, then cometary craters in the Orientale Basin could have formed during the time $\Delta t \approx \Delta T/15 \sim 0.3$ million years before the end of the last bombardment. Thus, the Orientale Basin age can be estimated at ~1 million years.

4. A weighty argument in favor of such a young age of the Orientale Basin, in our opinion, are also the smoothness of the bottom surface in central part of the basin (see Fig. 1), the incline of surface bottom, as well the different heights of the parapet surrounding the basin in its northern and southern part (see Fig. 2).

Conclusion The Orientale Basin was formed on the Moon not as a result of the fall of a large asteroid 3.8 billion years ago, but during the last bombardment of the Solar System by galactic comets of the Orion-Cygnus jet stream, at that this basin was formed at the very end of this bombardment.

In favor of the young age of the Orientale Basin, in our opinion, they say:

- Localization of this basin at the edge of the rock ejection zone from the South Pole-Aitken Basin;
- Multi-ring structure of the Orientale Basin with a displaced arrangement of the center of the rings;
- Low thickness of basalt lavas at the basin bottom;
- Low density of craters in the basin central part (Fig. 3).
- Relative smoothness of the basin bottom surface (Fig. 1).

We explain these facts by the basin origin of the not at the beginning of the cometary bombardment, but closer to its end. Thus, we believe that the Orientale Basin was finally formed ~1 million years ago and, therefore, is one of the youngest large impact structures on the Moon.

References

Barenbaum, A.A., 2010. Galaxycentric Paradigm in Geology and Astronomy, PH: Librokom, Moscow.

Barenbaum, A.A., 2015. Geological structures created by falls of galactic comets // Journal of Physics: Conf. Ser. 653. 012073, doi:10.1088/1742-6596/653/1/012073.

Barenbaum, A.A., 2019. Craters and seas on Mars and the Moon as a source of information about the flow of galactic comets in the Orion-Cygnus branch and the frequency of their fallout on the planets of the solar system // Proc. XX Int. Conf.: Physical-Chemical and Petrophysical Researches in the Earth's Sciences. Moscow, IGEM. P. 22-26.

Barenbaum, A.A. and Shpekin, M.I., 2011. About age of the lunar surface // Vestnik Otdelenia nauk o Zemle RAN, VOL. 3, NZ6011, doi:10.2205/2011NZ000141.

Barenbaum, A.A. and Shpekin, M.I., 2016. To the development of the mechanism of interaction of galactic comets with the terrestrial Planets // Journal of Physics: Conf. Ser. 774 012096, doi:10.1088/1742-6596/774/1/012096.

Barenbaum, A.A. and Shpekin, M.I., 2018. Problem of lunar mascons: an alternative approach // Journal of Physics: Conf. Ser. 946. 012079, doi:10.1088/1742-6596/946/1/012079.

Barenbaum, A.A. and Shpekin, M.I., 2018a. Cumulative formation of mares and mascons on Moon by galactic comets // Night Moscow Solar System Symp. 2018. IKI RAS. 9MS3-PS-81

Barenbaum, A.A. and Shpekin, M.I., 2019. Origin and formation mechanism of craters, seas and mascons on the Moon // Journal of Physics: Conf. Ser. 1147 012057. doi:10.1088/1742-6596/1147/1/012057.

Barenbaum, A.A. and Shpekin, M.I., 2019a. Origin of craters, mares and mascons on Moon in the light of the Galactocentric paradigm // Experiment in Geosciences. Vol. 25(1), p. 17–21.

Barenbaum, A.A. and Shpekin, M.I., 2019b. Problems of interpretation crater data in the Solar System // Tenth Moscow Solar System Symp., IKI RAS, 10MS3-PS-50.

Barenbaum, A.A. and Shpekin, M.I., 2019c. Origin of craters, seas and mascons on the Moon in the light of the Galactocentric paradigm // Proceedings of the All-Russian Annual Seminar on Experimental Mineralogy, Petrology and Geochemistry (VESEMPG-2019). Moscow, p. 261–265.

Barenbaum, A.A. and Shpekin, M.I., 2020. Cumulative hypothesis of formation on the Moon of the South pole-Aitken basin by galactic comets // Experiment in Geosciences. Vol. 26 (1), p. 11–15.

Barenbaum, A.A., and Shpekin, M.I., 2020a. The problem of the «South Pole-Aitken» basin formation // Eleventh Moscow Solar System Symp. IKI RAS. 11MS3-MN-PS-12.

Barenbaum, A.A. and Shpekin, M.I., 2021. Estimation of the flux density of galactic comets in the Orion-Cygnus branch based on number of shield volcanoes on Venus, craters on Mars and marine basins on the Moon // Journal of Physics: Conf. Ser. 1787, 012021, doi:10.1088/1742-6596/1787/1/012021

Barenbaum, A.A. and Shpekin, M.I., 2021a. On origin and age of mare Orientale on Moon // Twelfth Moscow Solar System Symp. IKI RAS. 2021, 12MS3-MN-PS-14.

Head J., Pieters C., Boardman J. et al., and M3 Team, 2009. Lunar Orientale Basin: Insights into Origin, Evolution and Crustal Structure from Chandrayaan-1 and Moon Mineralogy Mapper (M3) Data // MicroSymp. 50 "Vernadky-Brown", GEOKHI RAN, Moscow.

Johnson, B.C. et al., 2016. Formation of the Orientale lunar multiring basin // *Science.* Vol. 354, Is. 6311, p. 441–444.

Melosh, H.J., Freed, A.M., et al., 2013. The origin of lunar mascon basins // Science. Vol. 340, Is. 6140, p. 1552–1555.

Neukum, G., Ivanov, B.A., Hartmann, W.K., 2001. Cratering records in the inner Solar System in relation to the lunar reference system // Space Science Reviews, Vol. 96 (1-4), p. 55–86.

Zuber, M.T. et al., 2016. Gravity field of the Orientale basin from the Gravity Recovery and Interior Laboratory Mission // *Science*. Vol. 354, Is. 6311, p. 438–441.

Barenbaum A.A. Bombardments of Earth by galactic comets and supercontinental cyclicity. UDC: 551.1/4

Oil and Gas Research Institute of the Russian Academy of Sciences, Moscow (azary@mail.ru), tel: 8(499) 135-54-67

Annotation: A physical mechanism of supercontinental cyclicity is proposed, based on bombardments of Earth by galactic comets during the periods when Sun is in Galaxy spiral arms. Supercontinents are formed in Earth circumpolar zones at a very high density of galactic comet fallings, and cease to exist at mid-latitudes under conditions of a lower density of comet fallings. During periods of supercontinents formation, the axis of Earth's rotation always coincides in direction with the velocity vector of falling galactic comets. It was concluded that the reason for the cyclical supercontinents formation with a period of 400 Ma are the powerful bombardments of Earth by comets in the galactic arms, as well as the precession of Solar System ecliptic plane with a period equal to the rotation period of apsides line of Sun's orbit in Galaxy. Therefore, the supercontinental cyclicity should be explained by physical processes in Galaxy and Solar System, and not in the bowels of Earth.

Keywords: supercontinental cyclicity, galactic comets, galactic model

Introduction: It is known (Palin, 2020) that the formation of lithospheric plates and their association into supercontinents occurred on Earth starting from the Archean. In the geological history of the Earth, with varying degrees of reliability, 10 supercontinents have been identified today that arising with a period of T_{sk} = 400 Ma (Bozhko, 2009). In the life of each supercontinent, one can distinguish an assembly stage lasting ~150 Ma, when it is formed from relatively small plates, and a decay stage ~250 Ma, when it breaks up into parts. This disintegration could be complete or partial. In the latter case, the strongly disintegrated part found itself alternately either in the northern or in the southern hemisphere of the Earth. Therefore, the cyclic period can also be taken equal to 800 Ma (Bozhko, 2011).

A series of hypotheses has been proposed (Dien, 2019; Doucet, 2019; Palin, 2020), which try to explain the phenomenon of supercontinental cyclicity by the mechanism of lithospheric plate tectonics in various models of mantle convention. The main unresolved problem of all these hypotheses is the source of energy for the movement of plates and the physical mechanism that causes the plates to periodically form supercontinents in different hemispheres of the Earth.

Purpose of the article: In the early 2000s, we (Barenbaum, 2002, 2010; Barenbaum et al., 2002) developed a physical model that connects the cycles of global geological (biotic, climatic, and tectonomagmatic) processes on Earth with the Sun motion in the Galaxy and with bombardments of our planet by galactic comets at the times when Sun's entry into jet streams and spiral arms of the Galaxy. Optimization of this model (Barenbaum, 2018; Barenbaum, Titorenko, 2020) made it possible to build a high-precision geochronological scale common for the Phanerozoic and Neoproterozoic, to substantiate the "Snowball Earth" hypothesis for the supercontinent Pannotia (Barenbaum, 2021) in period of the Varanger glaciation, as well as clarify a number of important parameters of the Galaxy spiral structure.

It is shown below that this galactic model, which takes into account powerful bombardments of the Earth by galactic comets in the spiral arms of the Galaxy, also opens the way to understanding and studying the physical mechanism of supercontinental cyclicity.

Galactic model:

In the version of the model (Barenbaum, 2018), our Galaxy (Fig. 1) has 4 identical arms twisted in logarithmic spirals that rotate as a whole around the center with a period of T_G = 200 Ma, and 2 gas- dust jet streams twisted into an Archimedean spiral. Both streams consume at a speed of 300 km/s from the rapidly rotating gas and dust disk of Galaxy. The disk is inclined to the galactic side by an angle of 20° and precesses with a period of its revolution T_d = 50 Ma.

The intersections of jet streams with galactic arms are the main sites in Galaxy for the formation of young stars and comets. These processes are most active in the galactic arms at a distance of the corotation radius R* from Galaxy center, at which the radii of curvature of the jet streams and the galactic arms are equal.

From the moment of its formation in Crux-Scutum (IV) arm, Sun moves along an elliptical orbit, the line apsides of which rotates around Galaxy center with period $T_a = 2$ Ga. In this case, Sun either approaches the center at a distance of 5.27 Kpc, then recedes by R* = 11.47 Kpc, making low-amplitude oscillations across the galactic plane with a period $T_z = 50$ Ma.

This movement is in multifrequency parametric resonance (Molchanov, 1966; Barenbaum, 1998) with the rotation of galactic arms and Galaxy nuclear disk. So, for one complete revolution of the line apsides of its own orbit, Sun makes 8 orbital revolutions and 9 revolutions around galactic center, and Galaxy itself and its nuclear disk make 10 and 80 revolutions. In this case, Sun makes 80 oscillations across the galactic plane.

In the course of its movement, Sun episodically crosses galactic arms and jet streams, and at such times Earth and other planets of Solar System are bombardments by galactic comets. All these bombardments in the Earth geological history are the epochs of global natural catastrophes (biotic, climatic and tectonomagmatic), the times of which are clearly fixed by geologists in stratigraphic (geochronological) scale Phanerozoic in the form of its boundaries of different ranks (Fig. 2).

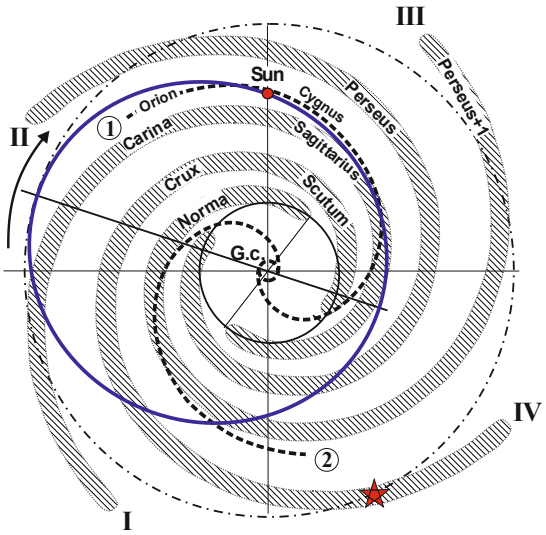

Fig. 1. The current position of the Sun (Sun) in orbit (ellipse) relative to 4 galactic arms (Roman numerals) and 2 jet streams (Arabic numerals) in projection onto the galactic plane. The small circle is the nuclear disk. The middle circle defines the Galaxy isothermal core. The outer dotted ring denotes the Galaxy corotation radius R*. The arrow is the direction of Sun's motion along its orbit and rotation of line apsides (straight line) of the orbit itself, which are coincided with the rotation of Galaxy and its nuclear disk. An asterisk is a place in the Crux-Scutum (IV) arm where the Solar System previously formed.

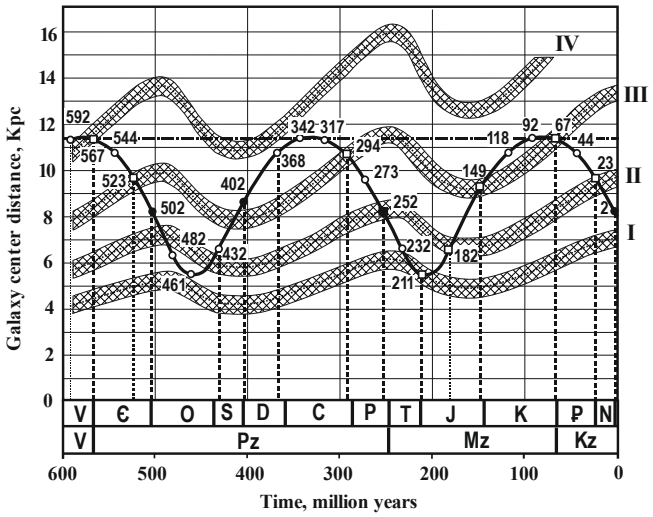

Fig. 2. Change in the Sun position in time relative to the galactic arms (bands) and its distance to Galaxy center (sinusoid) in projection onto galactic plane. Roman numerals are Galaxy arms numbers in Fig. 1. Figures show the time (million years) of Sun entering the jet streams (circles) and simultaneously in the galactic arms (squares). The black icons are the times when jet streams cross the galactic plane in which the Sun moves. The dashed-dotted line is the Galaxy corotation radius R*. Below is a time scale indicating boundaries of eras and systems of the Phanerozoic (Khain, 1982).

The model makes it possible to establish the average "width" of galactic arms, as well as to calculate the times of cometary bombardments with high accuracy, and thereby determine the age of the scale boundaries, starting from the rank of departments and above. It follows from the model that the most intense bombardments determine the boundaries of erathems and eras, the less intense bombardments determine the boundaries of systems, and the weaker ones determine the boundaries of departments. What is more, the department boundaries correspond to the Sun hitting only jet streams, the systems boundaries to the Sun hitting the jet streams and galactic arms simultaneously, and the era boundaries if that takes place in arms at a distance R* from Galaxy center. This case corresponds to the boundaries of Paleozoic (Pz) and Cenozoic (Kz) eras. For the Mesozoic (Mz), this condition is not met, and its boundary is considered to be a strong bombardment at the boundary of P and T systems (Fig 2).

Precambrian and Neoproterozoic scales: The patterns of alternation of strong cometary bombardments in Phanerozoic (Fig. 2) serve as the

basis (Barenbaum, 2010, 2021, 2021a) for studying the cyclicity of geological processes that occurred in Precambrian (Fig. 3) and, in particular, in Neoproterozoic (Fig. 4).

On fig. 3 shows a graph of the cyclicity of mega-events in the Earth geological history. It follows from it (Table 1) that all Precambrian mega-events were initiated by very powerful cometary bombardments that took place in the Galaxy arms at a distance R* from center. The bombardments were repeated with a period of T_B = 500 Ma, but their intensity differed in different arms. The most intense bombardments by galactic comets were in arm IV, weaker in arm II, and even weaker in arms I and III. We also see that arm Crux-Scutum (IV) is the site of two major cycles of planetary formation in the Solar System (Barenbaum, 2010).

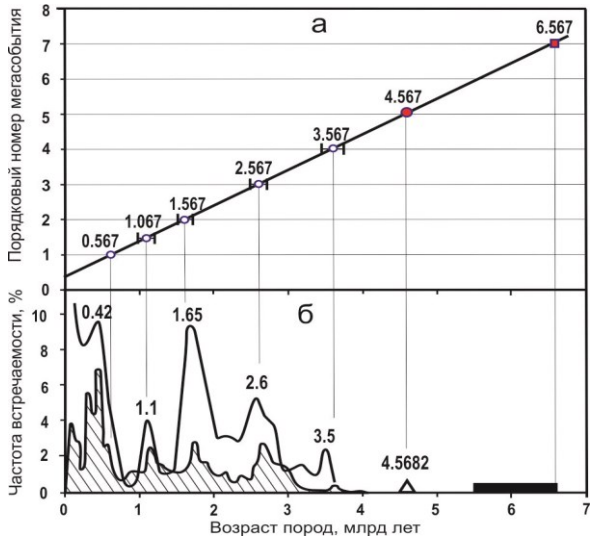

Fig. 3. a) Mega-events cycle schedule; b) curves is the activity of magmatism and ore formation processes (shaded) in the Earth history according to Pushkarev (1990). The parallelepiped is the age of iron meteorites of the Fe II class according to Sobotovich (1964). The triangle is generally accepted age of the Solar System formation.

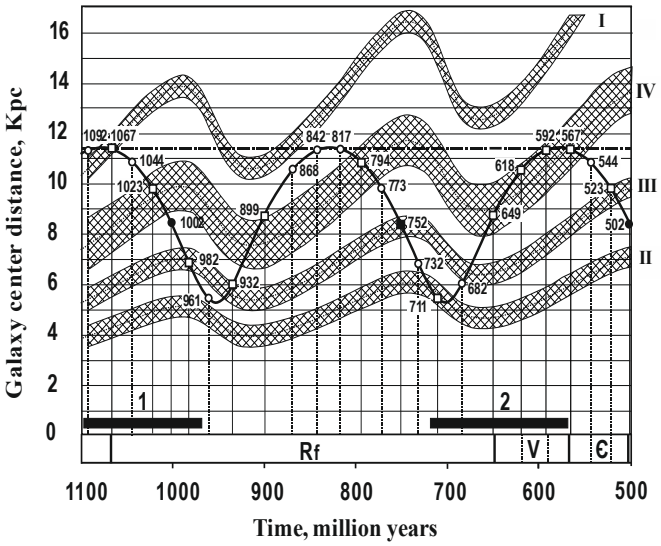

Fig. 4. The Sun position relative to the 4 arms of Galaxy in period from 1100 to 500 Ma ago. The Crux-Scutum (IV) arm width is 2 Kpc. The boundaries of Vendian, Cambrian, and Riphean correspond to the scale (Khain, 1982). At the bottom, the periods of supercontinents Rodinia (1) and Pannotia (2) existence are shown. All other designations (see Fig. 2)

Table 1: Relationship mega-events of Precambrian with galactic arms

Galactic arm	Event time, billion years	Precambrian eon and era boundaries (Plumb, 1991)
I. Carina-Sagittarius	1.067 3.067	Neoproterozoic -------
II. Perseus	1.567 3.567	Mesoproterozoic Paleoarchean
III. Norma-Perseus+1	2.067 4.067	------- Archaean (Eoarchean)
IV. Crux-Scutum	0.567 2.567 4.567 6.567	Phanerozoic (Paleozoic) Proterozoic (Paleoproterozoic) 2nd cycle of planet formation Solar System formation (Barenbaum, 2010)

Due to the resonant nature of Sun orbital motion in Galaxy, the Precambrian stratigraphic scale can be constructed according to the same rules as for Phanerozoic. An example of constructing such a scale for Neoproterozoic is shown in Fig. 4 (Barenbaum, 2021). Taking into account the data of geology, it is assumed in the calculation that arm IV is not only more powerful, but also "wider" than the other three Galaxy arms. In Vendian (Fig. 4), Sun moved inside this arm, so all cometary bombardments were strong. The bombardment 592 Ma ago was especially strong, and not much different from the bombardment 567 Ma ago at Vendian-Cambrian boundary. In stratigraphy, this boundary is also considered the Phanerozoic-Precambrian boundary, but its age has not yet been established. The calculation (Fig. 4) makes it possible to determine the exact age of this important boundary,

as well as to subdivide Riphean into 8 systems, including from 1 to 4 departments.

Glaciations and Supercontinents: Bombardments by galactic comets cause processes on Earth that can initiate both glaciations and the supercontinents formation. These processes (Barenbaum, 2010, Barenbaum, 2015; Barenbaum, Shpekin, 2016, 2019) are: 1) uplift of continents surface due to heating of asthenosphere rocks by cometary shock waves; 2) splitting of lithospheric plates and their migration; 3) bringing large amounts of water by comets; 3) evaporation of huge masses of water during comets falling into the ocean. As a result, during periods of strong cometary bombardment, powerful glaciers form on the continents, which partially or completely melt before the next bombardment (Barenbaum, 2010).

In (Barenbaum, 2021, 2021a), the author used this mechanism to explain the cause of a series of global glaciations (Table 2) that engulfed the Pannotia supercontinent (Fig. 4), which existed in the southern hemisphere of Earth at the end of Riphean and in Vendian.

Table 2: Periods of glaciations and moments of cometary bombardments

Glacial age (Chumakov, 2015)	Glaciation period, million years	Cometary bombardment, million years
1. Bayconur glaciation	547 – 542	544
2. Shuram-Wonoka Anomaly	–	592-567
3. Gaskiers glaciation	≈580	592-567
4. ?	614 ± 7	618
5. Marinoan glaciation	650 – 635	649
6. Glacial age (tentative)	685 – 667	682
7. Sturtian glaciation	715 – 680	711
8. Rapiten glaciation	730 – 710	732
9. Kaigas glaciation	754 – 746	752

Table 2 shows that the duration of these glaciations ranges from ≈1 to 35 Ma, and their onset almost coincides in time with cometary bombardments. We believe that the most probable reason for the formation of the Pannotia supercontinent and other supercontinents, as well as a number of glaciations (Table 2), were the bombardments of Earth by galactic comets during periods of time when the Earth's axis coincided in direction with the vector of comets motion.

The point is that on time scales of $\sim 10^8$–10^9 years, the orientation of Earth's rotation axis changes due to the precession of the ecliptic plane, in which Solar System planets move around Sun. In (Barenbaum et al., 2004), we tried to determine this precession period, which, according to our estimates, was T_E ~2700±500 Ma. At that time, it was not possible to measure the T_E value more accurately. Taking into account the features of supercontinental cyclicity allows solving this problem.

The existence periods of supercontinents according to the data of N.A. Bozhko (2011) in Fig. 5 are compared with the epochs of powerful cometary bombardments of Earth in the galactic arms (Table 1). It is clearly seen that supercontinents in its majority were formed and existed under conditions when Sun was in the galactic arms at a distance R* from the Galaxy center. Thus, the supercontinents Kenorland and Pannotia originated in a very powerful arm IV, Sebaquia and Gothia in arm II, and Vaalbara and Rodinia in arm I. The supercontinents Yatulia and Pangaea also originated in arm IV, but at a distance from the center R < R*.

In this regard, attention should be paid to the fact that the supercontinental cyclicity period T_S = 400 Ma does not coincide with either the period of Sun's orbital movement in Galaxy (Fig. 2) or with the period of strongest comet bombardments of Earth in the galactic arms T_B = 500 Ma (Table 1). As noted earlier, the main reason for this discrepancy is the change in orientation of Earth's axis due to the precession of Solar System ecliptic plane. Assuming the orientation factor of Earth's axis to be decisive, we find the value of precession period as $T_E = (T_S^{-1} – T_B^{-1})^{-1}$= 2000 Ma.

The obtained value T_E coincides exactly with the rotation period of the line apsides of solar orbit T_a. This means that in resonance with Galaxy rotation and its nuclear disk, not only the motion of Sun occurs, but also the precession of the ecliptic plane of Solar System. The main role in this phenomenon was played by the fall of galactic comets to the Earth, which alternately bombarded the southern and the northern hemispheres of the globe.

Our explanation for this phenomenon is that supercontinents form mainly in the circumpolar regions of the Earth due to a very high density of cometary falls, and break up in mid-latitudes at a

much lower density of cometary falls. Assuming that during the period of existence of Pannotia the Earth's axis was oriented strictly in the direction of comets motion, we come to the conclusion that Kenoria supercontinent must also have existed in the Southern hemisphere, and Sebakwia and Gothia supercontinents in the Northern one. The polar arrangement of these supercontinents is marked in Fig. 5 by icons (S) and (N). While the Vaalbara, Columbia and Rodinia supercontinents were supposed to be in low and middle latitudes.

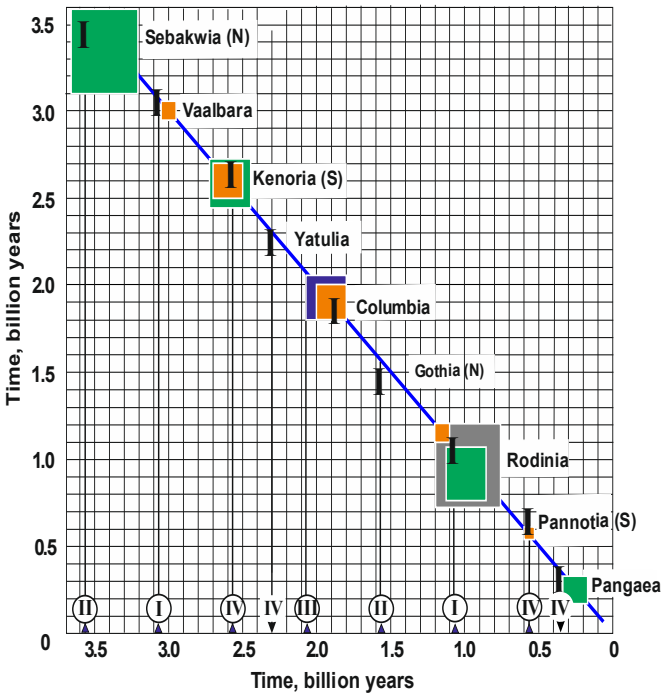

Fig. 5. Periods of the supercontinents existence (vertical axis) in comparison with times of cometary bombardments in the Galaxy arms (I – IV) at R = R* (circled) and R < R* (without circles). Black icons are data according to N.A. Bozhko (2011)

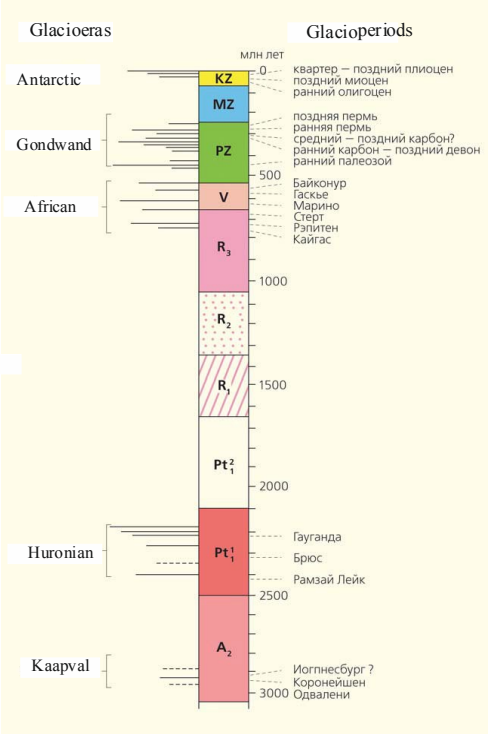

Fig. 6. Glacioeras and glacioperiods in interval from Late Archean to the present, according to N.M. Chumakov (2015). The long period of absence of glaciation between the Huronian and African glacioeras is the "Great Ice Pause"

Paleoreconstructions of all supercontinents well confirm these conclusions. At the same time, Vaalbara, Columbia, and Rodinia are at latitudes where, according to our model, they should decay rather than emerge. Therefore, their many faults and interior basins indicate that the Vaalbara, Columbia, and Rodinia never existed "as one" and therefore cannot be considered "supercontinents" in the strict sense of that definition.

Another important conclusion is that the scale and duration of glaciation is affected not only by the coincidence of the Earth's axis with the direction of movement of galactic comets, but also by the simultaneous the Sun presence in galactic arm of the Crux-Scutum (IV). The last two times when this condition was fulfilled, large global glaciations developed on the Earth (Fig. 6). The first of them ~2.5–2.2 Ga ago was called the Huronian glacioera, and the second ~750–540 Ma ago was called the African glacioera. Both glaciations occurred during the supercontinents location of in the Earth's Southern hemisphere: the Huronian glaciation developed on the Kenoria supercontinent, and the African one on the Pannotia supercontinent.

The time interval between these glaciations (see Fig. 6) is called the "Great Glacial Pause". During this "pause", according to the galactic model, the axis of the Earth never exactly coincided with the direction of the comets motion, as a result of which their bombardments of the Earth in galactic arms, although they created supercontinents, were much weaker than in the arm of Crux-Scutum (IV).

Conclusions

1. A physical mechanism of supercontinental cyclicity is proposed, based on bombardments of the Earth by galactic comets during the periods when the Sun is in the Galaxy spiral arms.

2. Supercontinents are formed in the Earth circumpolar zones at a very high density of galactic comet fallings, and cease to exist at mid-latitudes under conditions of a lower density of comet fallings.

3. During periods of supercontinents formation, the axis of Earth's rotation always coincides in direction with the velocity vector of falling galactic comets.

4. It was concluded that the reason for the cyclical supercontinents formation with a period of 400 million years are the powerful bombardments of Earth by comets in galactic arms, as well as the precession of ecliptic plane of the Solar System with the same period that the rotation of the line of apsides of Sun's orbit in Galaxy.

5. Therefore, supercontinental cyclicity should be explained by physical processes in Galaxy and the Solar System, and not in deep bowels of Earth.

References

Barenbaum A.A. 1998. Multifrequency parametric resonance in systems of satellites of giant planets // Proc. IV Cong. of Astronomical Society. Moscow. GAISH. MGU pp. 292–299. (In Russian).

Barenbaum A.A. 2002. Galaxy, Solar System, and Earth: Subordinate processes and evolution. – Moscow. PH: GEOS, 393 p. (In Russian).

Barenbaum A.A. 2010. Galactocentric paradigm in geology and astronomy. – Moscow. PH: LIBROKOM. 546 p.

Barenbaum A.A. 2018. Geological and meteoric data as a necessary tool for developing an adequate spiral model of the Galaxy // Proc. conf.: VESEMPG-2018. – Moscow. GEOKHI RAN. pp. 294–298. (In Russian).

Barenbaum A.A. 2021. Analysis of the causes of glaciations and δ13C anomalies of carbonates based on a galactic model // Proc. conf.: Fiziko-khimicheskiye i petrofizicheskiye issledovaniya v naukakh o Zemle. Moscow: IGEM RAN. pp. 22–26. (In Russian).

Баренбаум А.А. Подтверждение гипотезы «Snowball Earth» галактической моделью // *Геология морей и океанов.* Т.I. – М.: ИО РАН, 2021а. С.21-25.

Barenbaum A.A., Titorenko A.S. 2020. Galactic model of geological cyclicity: parameter optimization and testing based on geology and astronomy data // Proc. conf.: VESEMPG-2020. – Moscow. GEOKHI RAN. pp. 210–215.

Barenbaum A.A. Khain V.E., Yasamanov N.A. 2004. Large-scale tectonic cycles: analysis from the positions of the galactic concept // Vestnik Moskovskogo Universiteta. Geologiya, No.3, pp. 3–16.

Bozhko N.A. 2009. Supercontinental Cyclicity in the Earth's Evolution // Vestnik Moskovskogo Universiteta. Geologiya, No. 2, pp. 13–28.

Bozhko N.A. 2011. On Two Types of Supercontinental Cyclicity // Vestnik Moskovskogo Universiteta. Geologiya, No.5, pp. 36–61.

Molchanov A.M. Resonances in multifrequency oscillations // Doklady AN. 1966. Vol. 168, No.2. pp.284–287.

Chumakov N.M. 2015. Glaciation of the Earth: history, stratigraphic significance and role in the biosphere. – Moscow. PH: GEOS, 160 p. (In Russian).

Barenbaum A.A. 2015. Geological structures created by falls of galactic comets // J. Phys.: Conf. Ser. 653 012073.

Barenbaum A.A. and Shpekin M.I. 2016. To the development of the mechanism of interaction of galactic comets with the terrestrial planets // J. Phys.: Conf. Ser. 774. 012096.

Barenbaum A.A. and Shpekin M.I. 2019. Origin and formation mechanism of craters, seas and mascons on the Moon // J. Phys.: Conf. Ser. 1147. 012057.

Daiziel I.W.D. 1997. Neoproterozoic-Paleozoic geography and tectonics: Review, hypothesis, environmental speculation // GSA Bulletin. 109 (1): 16–42.

Dien H.G.E., Doucet L.S., Li. Z.-X. 2019.Global geochemical fingerprinting of plume intensity suggests coupling with the supercontinent cycle // Nature Communications. 10(1).

Doucet L.S., Li Z.-X., Ernst R.E. et al. 2019. Coupled supercontinent–mantle plume events evidenced by oceanic plume record // Geology. 48 (2). 159–163. DOI: 10.1130/G46754.1.

Palin R.M., Santosh M., Cao Wentao et al. 2020. Secular change and the onset of plate tectonics on Earth // Earth-Science Reviews. V. 207. 103-117.

Ivanov A.A.[1], Sevastyanov V.S.[1], Shnykin B.A.[1], Dolgonosov A.A.[1], Zevakin E.A.[1], Laurinavichus K.S.[2], Smirnova L.L.[3] Experimental model of organic compounds synthesis at prebiological stage of Earth using ultrasound generated by coastal sea pebles.

UDC: 550.47

[1]GEOKHI RAS, [2] IBPM RAS, [3] IPTS, Sevastopol.
aiva@geokhi.ru

Abstract. Experiments were carried out under natural and laboratory conditions to study effect of ultrasound, generated by coastal sea pebbles, on synthesis of organic compounds. Under natural conditions, the experiment was carried out on seashore, where tubular cuvettes made of aluminum and plastic 10 m long were installed, in which an aqueous solution of glycine was located. Under laboratory conditions, an aqueous solution of glycine and coastal sea pebbles were placed in a three-meter aluminum tube, vertically rotating at speed of 5 rpm, and also in a glass tube with the same filling, but rotating along its axis. In all cases, during the mechanical movement of the pebbles, ultrasound was generated, which, according to the idea of the experiment, should lead to formation of other organic compounds from glycine. According to results of mass-spectrometric analysis in aqueous solution of glycine in natural and laboratory conditions of the experiment, more complex organic compounds were found. This indicates real possibility of abiogenic synthesis of organic compounds in the coastal part of the Earth's primary ocean under the action of energy of sea waves.

Keywords: ultrasound; sea pebbles; glycine; abiogenesis; heterotrophic organisms.

Solution of the problem of abiogenic spontaneous generation of life largely depends on understanding the nature of self-organization of environmental conditions in which this became possible. Today we know that the conditions of abiogenesis should be

equally acceptable for the synthesis of polymeric organic compounds, and for the formation of prebiological structures from them, and, ultimately, for the appearance of protobionts. The cosmic position of the Earth allowed this process to take place and it remains to find a place that provided it with everything necessary for a geologically long period of time. For this purpose, we proposed to consider such a place as the caverns of the abrasion shores of the Earth's primary ocean. In the caverns, under the action of sea waves, a pneumatic shock occurred, due to which polypeptide microspheres could form from the primary broth, which was experimentally confirmed (Ivanov A.A., 2020; Ivanov A.A. et al., 2020). This is a very important result, since life begins with a cell, and a cell - with a shell that organizes the internal space for all its future contents, including nucleic acids, since not a single information structure in the form of nucleic acids is able to replicate without it. And today, not a single example of cell-free reproduction of creatures is known, even among the great species diversity of viruses that have highly organized DNA or RNA structures. Microspheres could change and, in fact, perform the function of cell membranes for protobionts. The active multiphase water-bubble medium of the caverns, due to regular changes in the pressure and temperature of their internal volume, made these microspheres pulsate to the beat of the sea surf, which, as expected, initiated the initial metabolism. And the vapor-phase condensate arising at the same time on the walls of the caverns contributed to the concentration of organic and inorganic compounds. Thus, the myriad of caverns of the abrasion shores of the Earth's primary ocean could work as mini laboratories, regularly cultivating and transforming the environment of abiogenesis.

In continuation of this work, we have obtained new research results that expand the range of ideas about the energy function of water in abiogenesis, while showing completeness of the problem of nature of the process, as well as the advantages of proposed approach, and the ways of its fundamental prospects. And what is fundamental – the question of the conditions for the formation of prebiological structures, is reduced to a number of restrictions that determine the possibility of preserving the native conformation of protein molecules, as the fundamental principle of the existence of all living organisms (Ivanov A.A., Galimov E.M., 2007). First of all, such limitations are determined by the temperature factor, the range of which is determined by the state of the liquid phase of water, and within which intracellular metabolism is possible. It follows from this that the abiogenesis medium of the structure-forming stage of the process must be formed in the same temperature range, which, in turn, obliges the previous stage – the stage of formation of organic polymers – to be within the same temperature limits. Otherwise, protein coagulation will occur. And this may mean that abiogenesis itself took place at temperatures of the liquid phase of water, and this, of course, requires appropriate approaches in the experimental modeling of such processes, subject to the continuity of the conditions for their occurrence. And this should continue until the appearance of heterotrophic organisms, otherwise, due to the exhaustion of the organic substrate, the process of development and evolution of life would not have continued. In this connection, our experimental studies are built according to the logic of these ideas, which predetermined the essence of this work, the idea of which is that the synthesis of organic polymers, and the formation of prebiological structures from them, should take place below the boiling point of water. However, an exception may be the conditions in which a short-term jump in pressure and temperature occurs, for example, as in the caverns of abrasive banks during a pneumatic impact (Ivanov A.A., 2020). In this case, due to the short duration of the process, the temperature of the total volume of the caverns remains within acceptable limits, and a significant jump in pressure and temperature occurs only in a microvolume of air bubbles dissolved in water.

So, the essence of our experiment is that the sea wave, moving the coastal pebbles, causes its particles to collide, which causes the generation of sound in a wide range, including in the ultrasonic frequency range, which is believed to facilitate the passage of chemical interactions (Margulis M. A., 1986). According to V.I. Bardyshev, recorded frequencies of ultrasound on the sea coast are in range from 20 to 800 kHz and higher (Bardyshev V.I., 2008). Considering all this, it was decided to experimentally establish whether ultrasound generated by coastal sea pebbles can initiate the condensation of glycine at temperatures lower than the boiling point of water. For this, tubular aluminum and plastic cuvettes 10 m long were installed on the sea coast, in which there was an aqueous solution of glycine. Part of each of the cuvettes was in the water, and part, for heating by sunlight, on the shore. Under laboratory conditions, an aqueous solution of glycine and coastal sea pebbles were placed in a three-meter aluminum tube, 10 cm in diameter, rotating vertically at a speed of 5 rpm, and also in a glass tube with the same filling, but rotating along its axis. A glass tube 115 cm long and 20 cm in diameter was heated in the center by a halogen lamp. At the same time, during the rotation of the pipe and its heating, a dry zone formed in the center, and moistened pebbles were distributed along its ends. Thus, in a glass tube rotating at an average

speed of 50 rpm, zones of wet pebbles were formed at the edges, where the temperature was from 20 to 30°C, and a central zone of the pipe with dry pebbles, which warmed up to 60°C. In all cases, during the mechanical movement of the pebbles, ultrasound was generated. After 2-3 days, within two weeks, water samples were taken from a glass pipe and the results of analysis for MALDI showed a gradual conversion of glycine to diglycine.

The mass spectrogram shows the conversion of glycine to diglycine by day of the experiment.

(From top to bottom: #1: 2 days, #2: 4 days, #3: 7 days, #4: 11 days, #5: 14 days, #6: matrix)

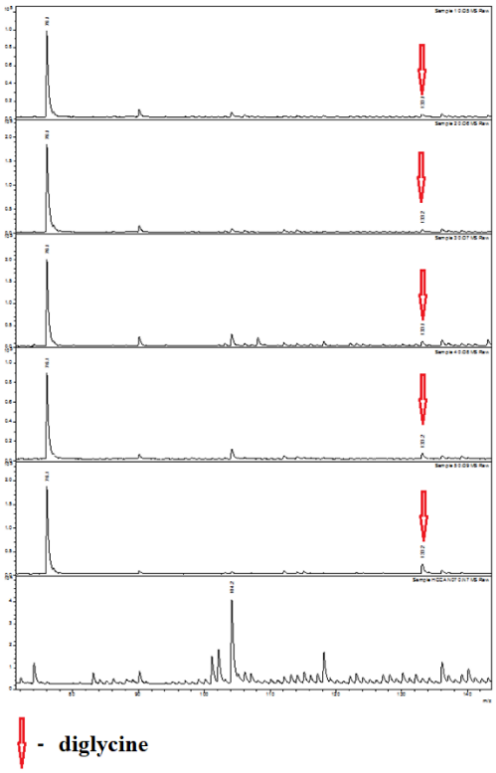

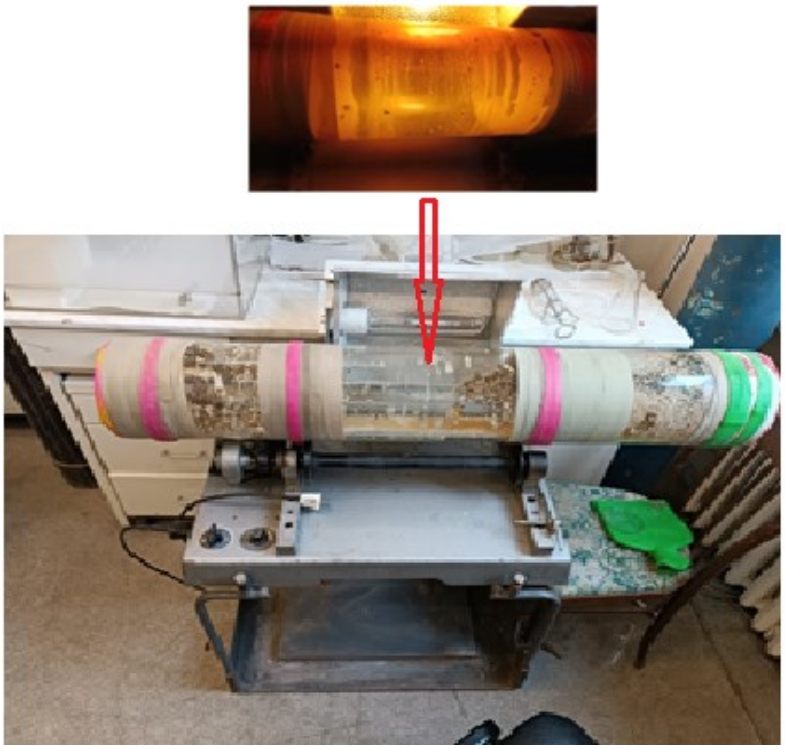

This experiment was carried out at pH-8.2, salinity - 35 ‰, gas composition of the experimental environment - N_2+CO_2 = 50×50%.

An experiment with a vertically rotating tube without heating did not reveal the presence of diglycine, but organic compounds more complex than glycine were found, the nature of which remains to be investigated, including at t = 60°C.

The experiment on the seashore with tubular cuvettes will continue for a year, but analysis of samples taken a month later from these cuvettes has already shown that a small amount of diglycine has appeared in an aqueous solution of glycine.

The first results of this experimental work show that ultrasound can influence the temperature regime of amino acid condensation, making it possible for this process to proceed within the temperature limits of the liquid phase of water, which corresponds to the criterion of the continuity of the conditions of the abiogenesis medium. This gives reason to believe that the processes of synthesis of organic polymers and the formation of prebiological structures from them are compatible, i.e. can take place in the same place at the same time. No less important is the fact that water, performing a new function, meets such possibilities of an ideal energy source as

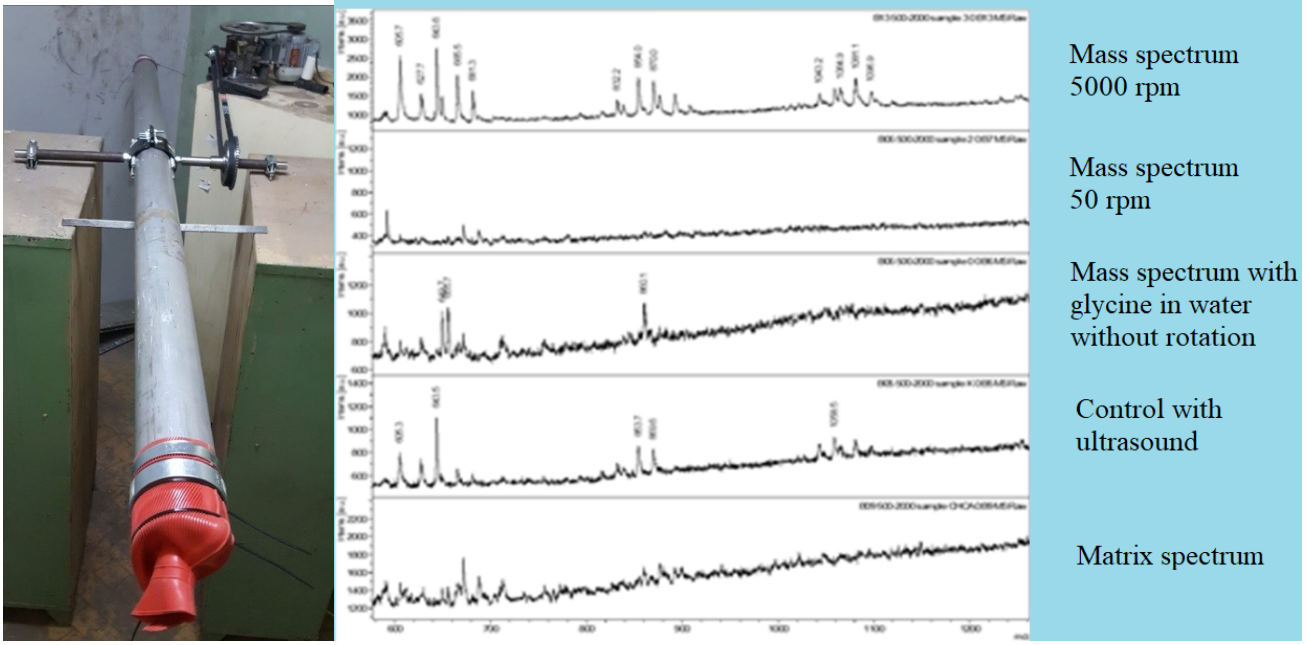

Installation of tubular cuvettes with glycine

- to be present on the early Earth;
- work in a cyclically operating mode;
- have sufficient but not excessive energy range;
- be in close proximity to the place of energy consumption;
- act around the clock both in winter and in summer, i.e. regularly day and night;
- the ability to work over a geologically long period of time;
- the ability to work simultaneously on land, at sea and in the primary atmosphere of the Earth;
- be able to transfer energy in a non-destructive, short-term and local way;

To all this is added the ability to regularly carry out the synthesis of polymeric organic compounds on the sea coast - the basis of all prebiological structures.

Funding: government assignment.

References

Bardyshev V.I. Underwater noises of the surf near the sea coasts of different types // Acoustic magazine. 2008. Volume 54, No. 6, p. 939-948.

Ivanov A.A. SHADOW STAGE OF ABIOGENESIS. The missing element of theories of the origin of life. M.: Publishing house IKAR, 2020.- 104 p.: ill

Ivanov A.A., Sevastyanov V.S., Shnykin B.A., Dolgonosov A.A., Krivenko A.P., Priymak S.V., Galimov E.M. Evaluation of the various energy sources effectiveness at the stage of prebiological structures formation during abiogenesis//Experiment in Geosciences 2020, Volume 26 N 1p.23-25

Ivanov A.A., Galimov E.M. Molecular isotopy of conformational interactions. Proceedings of the 18th Symposium on Geochemistry of Isotopes. Moscow. GEOKHI RAN. 2007 With. 106-108.

Margulis M.A., Fundamentals of sound chemistry, M., 1984; Sound-chemical reactions and sonoluminescence, M. 1986;

Tselmovich V.A.[1], Kurazhkovskii A.Yu.[1] Microstructure and composition of impact matter found when studying episodes of geomagnetic polarity change. UDC: 551.590.3

[1]Borok Geophysical Observatory, the Branch of Schmidt Institute of Physics of the Earth, Russian Academy of Sciences, Borok, Yaroslavl oblast, 152742 Russia
tselm@mail.ru, ksasha@borok.yar.ru тел. +7(9066327448)

Abstract. According to the hypothesis of A.A. Barenbaum (Barenbaum, 2010), changes in the fluxes of cosmic matter to the Earth can determine the mode of changes in the polarity of the geomagnetic field. We made an attempt to find a relationship between the behavior of the geomagnetic field and variations in the intensity of the influx of cosmic dust onto the Earth's surface. The dynamics of the influx of cosmic matter and its correspondence to the regime of geomagnetic inversions was studied on the deposits of the Upper Cretaceous – Lower Paleogene, in the coastal outcrop of the river Volga (Mount Syrt), at the point with coordinates (50°43.001° N, 45°38, 408° E). We found that the time of formation of sedimentary horizons with high concentrations of native metal particles coincided with short-term episodes of geomagnetic polarity disturbance. This confirms the possibility of the existence of a correlation between the intensification of cosmic dust flows and short-term polarity changes (excursions) of the geomagnetic field.

Keywords: geomagnetic polarity, impact event, native metals.

Introduction. The concentration of native metal (NM) particles in sedimentary rocks is usually low and largely determined by the background input of cosmic dust. At the same time, it is known that their concentration can increase in areas of activation of basalt (Markov et al., 2019) or explosive (Grebennikov et al., 2012) magmatism (mainly Fe particles) in areas where meteorites fall (Feldman et al., 2018).), as well as due to an increase in the density of cosmic dust fluxes entering the earth's surface. It should be noted that igneous rocks containing SM particles are extremely rare (Markov et al., 2019). In this regard, the enrichment of sedimentary rocks with SM particles (Fe, Ni, etc.) in regions remote from areas of active tectonic and magmatic processes is usually associated with cosmic events. Thus, a high concentration of SM particles in sediments corresponding to the Cretaceous-Paleogene boundary is associated with the fall of a large meteorite. The thickness of the horizon enriched in SM particles, which is taken to correspond to the Cretaceous–Paleogene boundary, usually does not exceed a few mm (Grachev et al., 2005; Sungatullin et al., 2016; 2018).

Methods and results. In the deposits of the Upper Cretaceous - Lower Paleogene, we found three horizons enriched with SM particles, the thickness of which was about 1 m. It is unlikely that the existence of horizons of such a thickness can be associated with meteorite falls. Two horizons containing an increased amount of SM belonged to the deposits of the Upper Campanian, one horizon was formed in Denmark. The data shown in Figs. 1–6.

Fe and Ni particles and magnetite spherules were found most frequently in these horizons. In addition, particles of Ag, Zn, Cu, W and small metal spheres were detected. SM particles can be conventionally divided into two groups: large (of the order of 10–50 μm) and small (of the order of 1 μm). We did not find fundamental differences between the quantity and mineralogical composition of large (10–50 μm) SM particles from the Upper Cretaceous and Lower Paleogene deposits. The number of small metallic spherical particles in the Cretaceous and Paleogene deposits differed. The maximum number of small spherical particles was found in the Paleogene deposits (Fig. 1). In accordance with estimates of the rates of marine sedimentation, the duration of the formation of these horizons could be tens of thousands of years.

It is rather difficult to identify with certainty the reason for the increase in the amount of SM in the studied horizons. For this, both cosmogenic and exogenous hypotheses can be involved. In this case, the cosmogenic genesis of an increase in the concentration of SM particles seems to us more probable. To substantiate the nature of the increased concentration of SM particles in the studied sediment horizons, the following arguments can be used. In some cases, the composition and shape of cosmogenic and terrigenous dust particles can be practically indistinguishable. First of all, this refers to the presence of magnetite spherical particles (Tselmovich et al., 2022) and elongated particles of native flake iron (Markov et al., 2019). Such particles can have both undoubtedly terrigenous (in tuffs and mafic lavas) and cosmic (in regolith) genesis. At the same time, it should be noted that the area of the studied deposits is significantly (more than 1000 km) removed from the areas in which magmatism activation took place. The transfer of a large number of large SM particles over such distances is unlikely. The cosmic genesis of SM particles is evidenced by their mineral composition, which largely coincides with the composition of the background cosmic dust previously studied by us in peat strata of the Holocene age. In addition, it is traditionally assumed that the presence of Ni particles and its compounds with iron is an argument in favor of the cosmogenic nature of SM particles (Grachev, 2010).

Conclusions. In the course of this study, we determined the behavior of the direction of remanent magnetization of samples selected according to the thickness of the studied sedimentary strata. At the same time, it was found that the direction of magnetization of horizons enriched with SM particles

on average by more than 90º differed from its direction in horizons in which the concentration of SM particles was low. Such a coincidence of sharp changes in the direction of magnetization with sharp changes in the SM concentration gives grounds for the assumption that the passage of our planet through relatively dense cosmic dust flows can significantly affect the behavior of the main geomagnetic field. According to our estimates, the duration of the anomalous behavior of the main geomagnetic field associated with the impact of cosmic dust flows can reach several tens of thousands of years. This is much less than the duration of polarity chrons, which are taken into account in the geomagnetic polarity scales. Thus, we have found cases of a correlation between the intensification of cosmic dust flows with geomagnetic events belonging to the class of geomagnetic excursions.

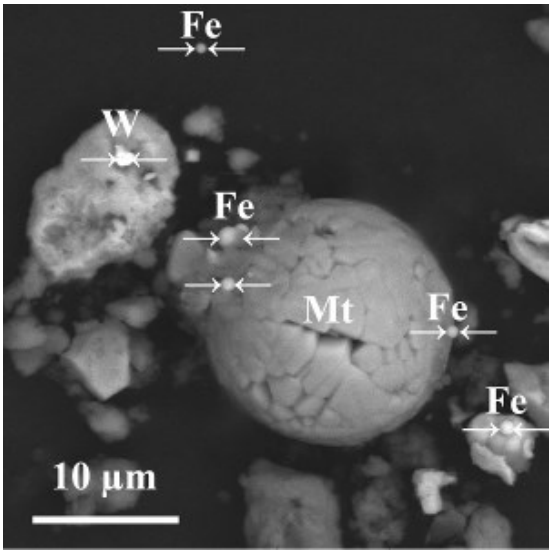

Fig.1. Native iron balls on a magnetite ball, native W.

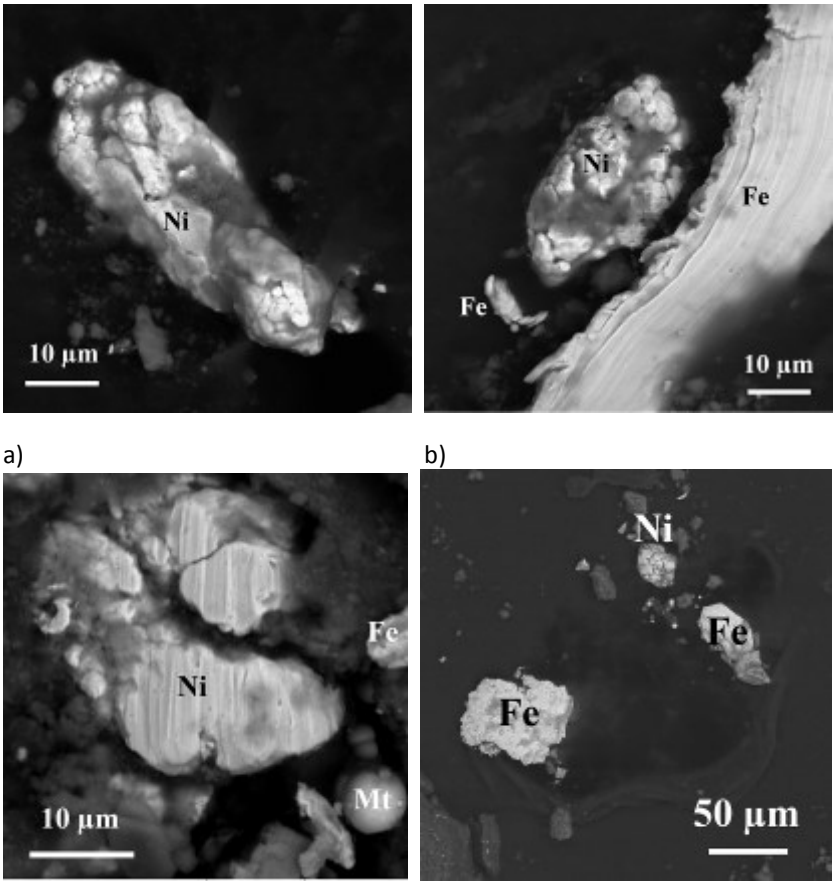

Fig.2. A particle of native nickel (a,b,c,d), iron (b,c,d) and Mt microsphere (c).

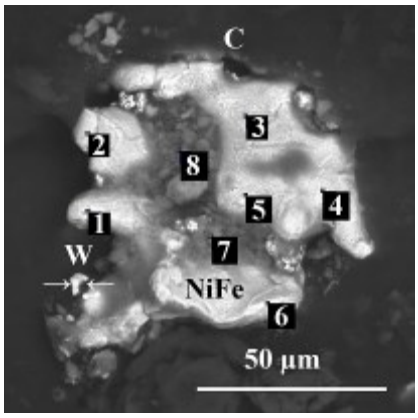

Fig.3. FeNi alloy, 1-8 – points Variable composition

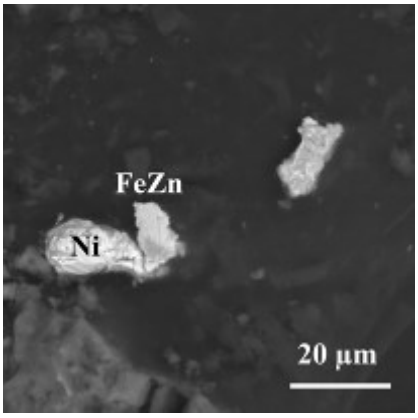

Fig.4. Alloy of FeZn and Ni

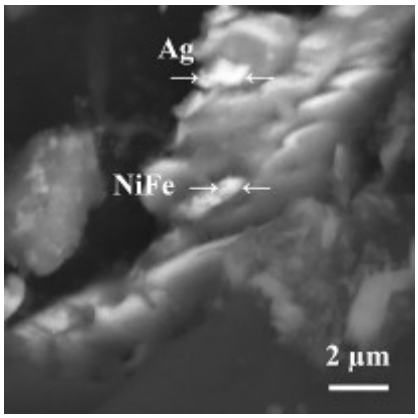

Fig.5. Ag and NiFe

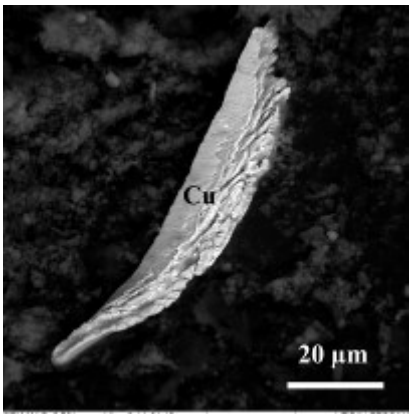

Fig.6. Cu particle

The work was done according to the state task of GO BOROK IPPE RAS, microprobe - RFBR 16-05-00703a

References

1. Barenbaum A.A. A new approach to solving the problem of paleomagnetic reversals. Proceedings of the Eleventh International Conference "Physical-Chemical and Petrophysical Research in the Earth Sciences". Moscow 11-13, Borok October 14, 2010. P. 40–43.
2. Grachev A.F. To the question of the nature of cosmic dust in sedimentary rocks // Physics of the Earth. 2010. No. 11. P. 3–23. 3.

Grebennikov A.V., Shcheka S.A., Karabtsov A.A. Silicate metal spherules and the problem of the mechanism of ignimbrite eruptions (on the example of the Yakuta volcano-tectonic structure). // Volcanology and seismology. 2012. No. 4. S. 3–22.

4. Markov G.P., Pechersky D.M. Omnipresent iron. Moscow: Geos, 2019. 129 p.
5. Sungatullin R.Kh., Tselmovich V.A., Vafin R.A., Sungatullina G.M. Geomorphological and geological-mineralogical signs of the impact origin of the Rabiga Kul lake basin, Republic of Tatarstan // Geomorphology. 2016. No. 1. S. 64–72.
6. Sungatullin R.Kh., Bakhtin A.I., Tselmovich V.A., Bakhmutov V.G., Sungatullina G.M. Middle Paleozoic impact event in the southwest of the East European Platform. // Geology and geophysics. 2018. V. 59. No. 9. S. 1431–1444
7. Feldman V.I., Glazovskaya L.I. Impactogenesis: study. allowance. M. Publishing house: KDU, 2018. 151 p.
8. Tselmovich V.A., Maxe L.P. Microstructure and composition of magnetic microspheres of anthropogenic and cosmogenic origin. All-Russian annual seminar on experimental mineralogy, petrology and geochemistry (VESEMPG-2022), April 19–20, 2022 Abstracts. GEOKHI, Moscow 2022. P. 131.
9. Grachev A.F., Korchagin O.A., Kollmann H.A., Pechersky D.M, Tselmovich V.A. A New Look at the Nature of the Transitional Layer at the K/T Boundary near Gams, Eastern Alps, Austria, and the Problem of the Mass Extinction of the Biota // Russian Journal of Earth Sciences. 2005 Vol. 7. No. 6. P. 1–45.

Kuyunko N.S. The researches of meteorites by thermoluminescent method. UDC: 550.42

Vernadsky Institute of Geochemistry and Analytical Chemistry RAS, Moscow (ninakuyunko@gmail.com)

Abstract. The most significant results of our investigation of meteorites by the thermoluminescent method are presented. The values of natural (accumulated in outer space) and induced in laboratory conditions from an

external radioactive radiation source thermoluminescence of meteorites of various chemical classes were used to evaluate orbits, analyze the effects of shock-thermal metamorphism, and identify finds of unknown genesis. In nonequilibrium ordinary and carbonaceous chondrites, the sensitivity of induced thermoluminescence makes it possible to reliably subdivide weakly metamorphosed meteorites (type 3) into subtypes 3.0-3.9. The temperature of the maximum of the peak of thermoluminescence and its width carry information related to the thermal history. A method for identifying extraterrestrial matter by the ratio of natural and X-ray induced thermoluminescence is proposed. The dependence of the peak height and the intensity of the thermoluminescent glow on the shock class of equilibrium ordinary chondrites is established and the magnitude of the shock load is calculated.

Keywords: thermoluminescence; meteorites; shock metamorphism.

The thermoluminescent method is successfully used to study the substance of meteorites. Under the influence of cosmic radiation, in addition to cosmogenic isotopes, traces of radiation disturbances accumulate in the mineral components of meteorites, which cause thermoluminescent glow when the substance is heated. The thermoluminescent method is one of the simplest and most reliable methods for registering structural changes in a substance. It is widely used for meteorite research. Measurements of natural thermoluminescence (stored by a meteorite in outer space) are mainly used to assess the orbits of meteorites, to analyze impact metamorphism, to assess the terrestrial ages of meteorites, to identify the effects of environmental effects on the meteorite substance and to identify paired samples-finds. Measurements of induced thermoluminescence are used to study the metamorphism of ordinary and carbonaceous chondrites, as well as to study the shock-thermal history of meteorites.

This paper presents the most significant results of our investigation of meteorites by the thermoluminescent method. Measurements of natural and laboratory-induced from an external radioactive radiation source thermoluminescence of meteorites of various chemical classes were performed.

For research, gross samples of meteorites weighing 0.7-1.0 g were crushed and crushed in a jasper mortar under a layer of ethyl alcohol. The magnetic fraction was separated with a hand magnet after drying for 24 hours in air. Three samples weighing 2 mg were prepared from the nonmagnetic fraction of each test sample by quartization method. Each sample was placed in a 6 mm diameter beryllium foil dish and evenly distributed on the bottom with an acetone drop under the binocular. The solvent was removed by air-drying for 24 hours. Thermoluminescence was recorded on a modified laboratory unit. The interface made on the basis of the L-154 board made it possible to register the photomultiplier current and the sample heating temperature on a computer. The resolution of the registration was 1°C. The thermoluminescence intensity was calculated relative to the Dhajala 3.8 chondrite. The average value of three measurements was used to calculate the thermoluminescence parameters.

Thermoluminescent studies (Sears, 1988, Sears, 1991, Guimon, 1995) have shown that nonequilibrium ordinary and carbonaceous chondrites constitute a metamorphic sequence. The peak height and the area under the thermoluminescent glow curve in the temperature range of 50-350°C were considered as indicators of the degree of metamorphism (Kuyunko et al., 2015). In addition, the glow curves were approximated by a Gaussian curve and the termoluminescence intensity was determined both in total and in different temperature intervals. The calculations performed by us showed the consistency of the results both using the peak height and the area in different temperature intervals of the approximated Gaussian thermoluminescent curve, and using the original thermoluminescence spectrum. Therefore, further calculations of thermoluminescence parameters were carried out according to the initial spectrum.

Measurements of thermoluminescence induced by X-ray radiation in laboratory conditions for ordinary nonequilibrium chondrites allowed us (Kuyunko et al., 2015) to establish the correlation dependence of induced thermoluminescence with the petrological subtype in the range 3.0-3.9 and use it for the classification of samples-finds.

The glow curves of X-ray induced thermoluminescence of carbonaceous chondrites have a complex shape with a peak in the temperature range of 100-130°C (Kuyunko et al., 2020). In some samples, less pronounced peaks are recorded at temperatures above 150°C. According to the intensity of the glow at the low-temperature peak of thermoluminescence spectrum (up to 130°C), 10 subtypes 3.0-3.9 can be distinguished in carbonaceous chondrites of the CO and CV type, similar to ordinary nonequilibrium chondrites, reflecting the degree and nature of metamorphism of their parent bodies. Figure 1 shows the relationship between the height of the low-temperature peak and the intensity of laboratory-induced X-ray radiation thermoluminescence with the petrological subtype of the carbonaceous chondrites studied.

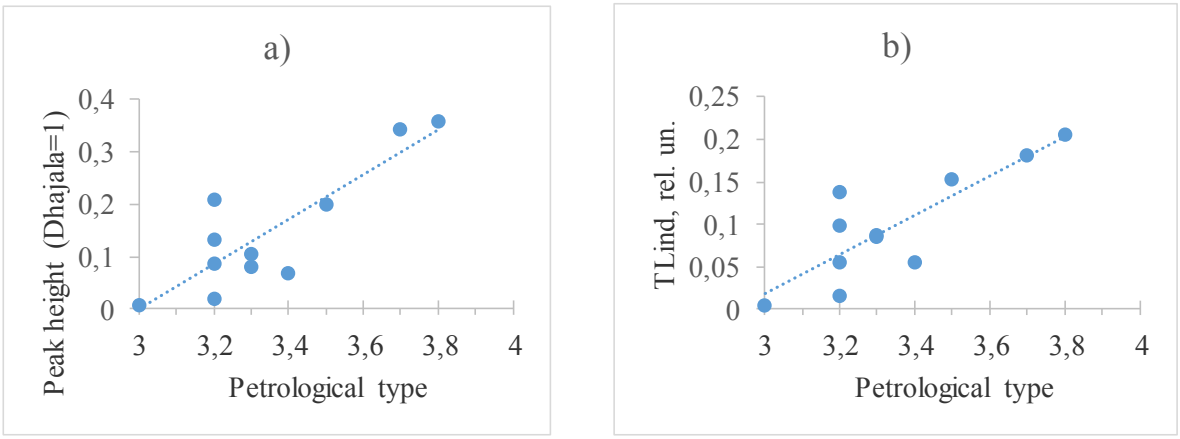

Fig. 1. Dependence of peak height (a) and intensity of induced thermoluminescence TLind (b) on the petrological type of carbonaceous CV and CO group chondrites.

Induced thermoluminescence (induced from an external radioactive radiation source under laboratory conditions) reflects changes in the crystal structure of feldspar as a result of thermal or shock-induced metamorphism. The most severely impacted ordinary chondrites, in which feldspar has been melted or partially converted into maskelenite, have a thermoluminescence sensitivity one or two orders of magnitude lower than unpaired equilibrium chondrites. Our measurements (Ivliev et al., 1995, 1996, 2002) of thermoluminescence stored under X-ray irradiation in laboratory conditions in samples of oligoclase, quartz calcite subjected to experimental shock loading showed significant changes in the intensity of thermoluminescent glow. This circumstance allowed us to conclude that the observed variations in the intensity of thermoluminescence are mainly due to different degrees of shock metamorphism.

It was found (Ivliev et al., 2007, Kuyunko, 2021) that the height of the peak and the area under the curve of the thermoluminescent glow depend on the impact class of meteorites. However, the height of the peak of the glow and the area under the curve of the thermoluminescent glow in the temperature range of 50-350°C, obtained by X-ray irradiation of meteorite samples in laboratory conditions, turned out to be more sensitive indicators of the degree of collision. As follows from Fig. 2, when the shock pressure increases to 10 GPa (stages S1-S2), the values of the peak height of the glow and the intensity of thermoluminescence increase, and then sharply decrease to two orders of magnitude with a further increase in the shock pressure from 10 to 90 GPa (stages S3-S5).

The thermoluminescent method was used by us (Kuyunko et al., 2019) to identify extraterrestrial matter. In order to establish criteria for the identification of a substance of extraterrestrial origin, measurements of natural and X-ray induced thermoluminescence in laboratory conditions were performed for a large group of meteorites of various chemical classes and samples of unknown genesis received by the GEOCHI RAS from the population.

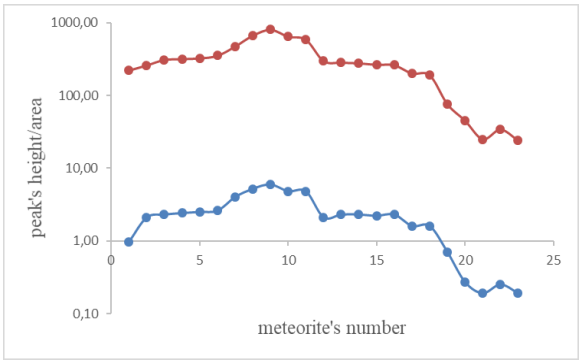

Fig. 2. The dependence of the peak's height (blue curve) and the area under of the thermoluminescent glow curve (red curve) on the meteorite's shock classes.

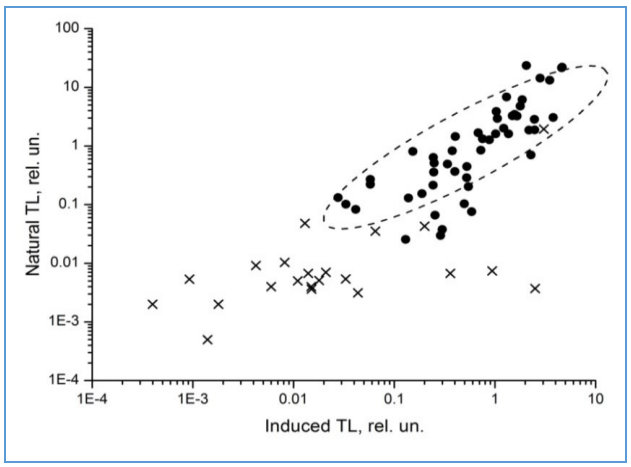

Fig. 3. The ratio of the natural and X-ray induced thermoluminescence in chondrites (circles) and in samples of uncertain origin (crosses).

It should be noted that for samples of unknown origin, the characteristics of the thermoluminescence spectra – the position of the peak maximum, its width, and the shape of the curve differ significantly from the corresponding characteristics of the Dhajala H3.8 chondrite and other meteorites. A region with a positive correlation between natural and X-ray induced thermoluminescence has been identified for meteorites (Fig.3). Samples of unknown genesis do not belong to this region. For them, the value of natural thermoluminescence is significantly lower than the value expected for the measured values of induced thermoluminescence in these objects, when compared with data for meteorites. Two samples are located on the boundary of the meteorite region, they are characterized by higher values of natural and X-ray induced thermoluminescence. However, the shape of the spectrum of natural thermoluminescence does not allow them to be attributed to objects of cosmic origin. Higher values of natural thermoluminescence may be due to their technogenic origin, and a significant content of feldspar has led to an increase in the level of induced thermoluminescence.

Thus, the algorithm for identifying finds of unknown genesis is reduced to measuring natural and X-ray-induced thermoluminescence according to the above methodology and determining by their ratio whether they belong to the meteorite region. The shape of the thermoluminescence spectrum, the position of the peak maximum, and its width are additional arguments for identifying samples of extraterrestrial origin.

Conclusions. The most significant results of the study of meteorites by the thermoluminescent method are presented. In nonequilibrium ordinary and carbonaceous chondrites, the correlation dependence of X-ray induced thermoluminescence with the petrological subtype in the range 3.0-3.9 has been established, allowing it to be used for the classification of samples-finds. A method for identifying extraterrestrial matter by the ratio of natural and X-ray induced thermoluminescence is proposed. The dependence of the peak height and the intensity of the thermoluminescent glow on the shock class of equilibrium ordinary chondrites is established and the magnitude of the shock load is calculated.

The work was carried out within the framework of the budget topic of the Vernadsky Institute of Geochemistry and Analytical Chemistry of the Russian Academy of Sciences.

References

Ivliev A.I., Badyukov D.D., Kashkarov L.L. (1995) Studies of thermoluminescence in samples subjected to experimental shock loading. Me: Oligoclase. Geochemistry. No. 9. pp. 1368-1377.

Ivliev A.I., Badyukov D.D., Kashkarov L.L. (1996) Studies of thermoluminescence in samples subjected to experimental shock loading. II: Quartz. Geochemistry. No. 10. pp. 1011-1018.

Ivliev A.I., Badyukov D.D., Kuyunko N.S., Kozlov E.A. (2002) Studies of thermoluminescence in samples subjected to experimental shock loading. III: Calcite. Geochemistry. No. 8. pp. 820-833.

Kuyunko N.S., Ivliev A.I., Alekseev V.A. (2015) Determination of the degree of metamorphism of ordinary nonequilibrium chondrites by thermoluminescent method. Proceedings of VESEMPG-2015, 1, 293-296.

Kuyunko N.S., Alekseev V.A. (2019) Method of identification of extraterrestrial matter by thermoluminescent characteristics. Proceedings of VESEMPG-2019, 293-296.

Kuyunko N.S., V. Alekseev.A. (2020) Thermoluminescent studies and determination of the degree of metamorphism of carbonaceous chondrites together and summary. Proceedings of VESEMPG-2020, 255-258.

Kuyunko N.S. Thermoluminescent properties of equilibrium byknovennyh chondrites of various shock classes. Proceedings of VESEMPG-2021, 198-201.

Gaimon R.K., Simes S.I., Derek W.G. et al. (1995) Chemical and physical studies of Type XII chondrites 3: Metamorphic history of CV chondrites and their components. Meteoritics. V.30. N6. P.704-714.

Ivliev A.I., Alekseev V.A., Kuyunko N.S. (2007) Investigation of shock metamorphism of ordinary chondrites by thermoluminescence. Lunar Planet. Sci. 38, Houston: LPI, CD#1043.

Sears D.U.G., Grossman J.N., Melcher K.L. et al. (1980) Measurement of the metamorphic history of nonequilibrium conventional chondrites. Nature, 287 (5785), 791-795.

Sears D.W.G., Batchelor J.D., Lu J., Keck B.D. (1991) Metamorphism of CO and CO-like chondrites and comparison with ordinary type 3 chondrites. Proc. A symptom of NIPR. Antarctica. Meteorites, 4, 319-343.

Lavrentjeva Z.A., Lyul A.Yu. The trace element studies of grain-sized fractions from ATLANTA EL6 equilibrated enstatite chondrite. UDC: 552.63

V. I. Vernadsky Institute of Geochemistry and Analytical Chemistry RAS, Moscow (lavza@mail.ru).

Abstract. This paper presents the results of trace element abundances in magnetic and nonmagnetic size

fractions from enstatite chondrite Atlanta EL6. It is assumed that some features of the distribution of lithophilic and siderophilic trace elements were acquired as a result of crystallization of impact melts. The origin of such melts could be as a result of impact melting in situ or impact melt ejections.

Keywords: enstatite chondrites, mineral fractions, abundance of microelements.

Mineralogical and isototopic data indicate that enstatite chondrites formed in a nebular region distinct from the other main belt asteroids possibly in the inner part of the solar system [Kallemeyn and Wasson, 1986; Shukolyukov and Lungmair,1998]. Enstatite chondrites are thought to have formed in highly reducing environment. This inference is supported by the high Mg/(Mg + Fe) of olivine and pyroxene, presence of Si in Fe,Ni metal, and occurrence of typically lithophile elements, such as Ca, Mg, Mn and K, in sulfide minerals in enstatite chondrites [Weisberg et al., 2009]. Enstatite chondrites are divided into two main groups, EH and EL, based on high and low abundances of Fe,Ni metal: both groups show a metamorphic sequence from type 3 to 6 similar to that observed in ordinary chondrites [Baedecker и Wasson, 1975 и Sears, 1980]. The Atlanta meteorite is classified as an EL6 enstatite chondrite. Meteorites of the EL group are well crystallized and practically do not contain chondrules, but belong to chondrites due to the similarity of chemical and mineralogical compositions. The meteorite is a breccia containing centimeter-long clasts rich in troilite embedded in a recrystallized chondrite matrix. The clasts and matrix are composed of the same minerals, differing only in the content of troilite (Petaev and Skripnik, 1983). In order to obtain more information about the features of the composition of the EL group of chondrites, to evaluate the influence of nebular fractionation and metamorphism, in the non-magnetic and magnetic size fractions of the enstatite chondrite Atlanta EL6, the contents of trace elements were determined by the INNA method and their distribution in the material of the studied meteorite was analyzed.

Samples and methods. The fractions were obtained by sorting the samples according to the grain size by the granulometric method and manually under a microscope. Determination of the contents of elements in fractions was carried out at the Central Laboratory for the Analysis of Substances of the Geochemical Institute of the Russian Academy of Sciences using an optimized version of instrumental neutron activation analysis. The method was developed for the analysis of extraterrestrial matter [Kolesov et al., 2001].

Results and its discussion. The features of the microelement composition of granulometric fractions isolated from the equilibrium enstatite chondrite Atlanta EL6 are considered (Tables 1, 2). All non-magnetic fractions in the Atlanta meteorite are depleted in light REE relative to heavy ones - $[(La/Lu)_F / (La/Lu)_{CI}] = 0.5 – 0.8$ and have both positive and negative Eu anomalies - $[(Eu/Sm)_F / (Eu/Sm)_{CI}] = 0.6 – 1.5$. The main part of rare earth elements was concentrated in non-magnetic fractions with a grain size of $1<d<45$ μm. The concentrators of rare earth elements, apparently, are accessory minerals, which are most enriched in ultrafine fractions. (Fig.1.)

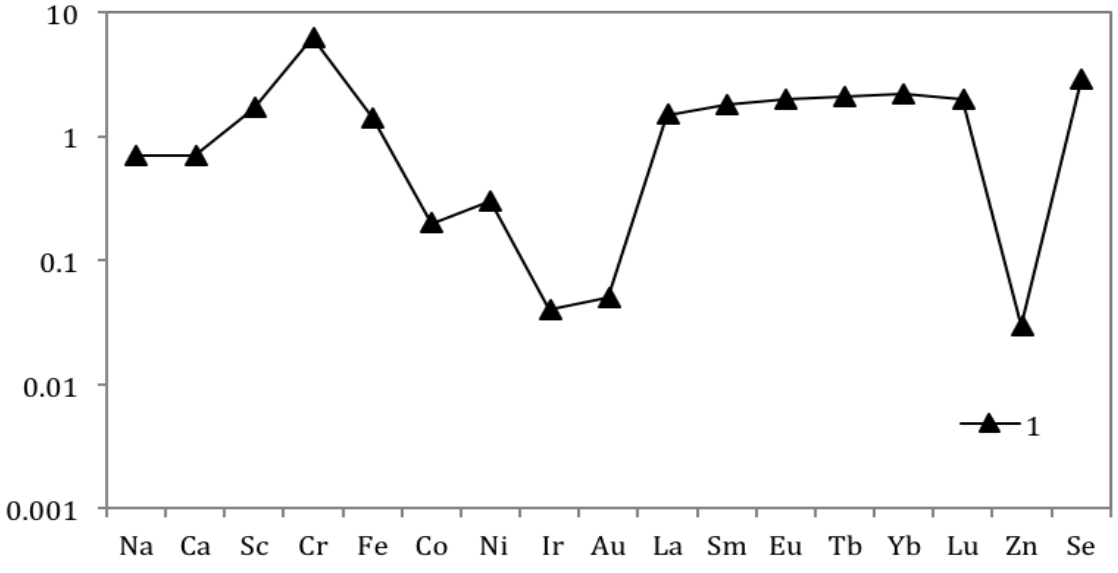

Fig. 1. Element contents normalized to CI chondrites in the "fine-grained" non-magnetic fraction ($1<d < 45$ μm) from Atlanta enstatite chondrite.

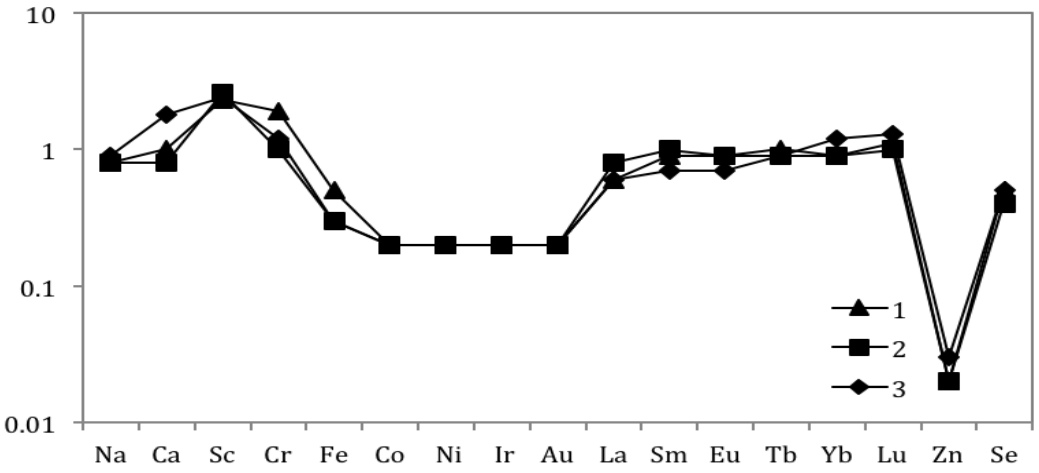

Fig. 2. Normalized to CI chondrite element contents in "medium-grained" non-magnetic fractions from Atlanta enstatite chondrite. 1 – (45<d <71 μm); 2 – (1<d<100 μm); 3 - (100<d<160 μm).

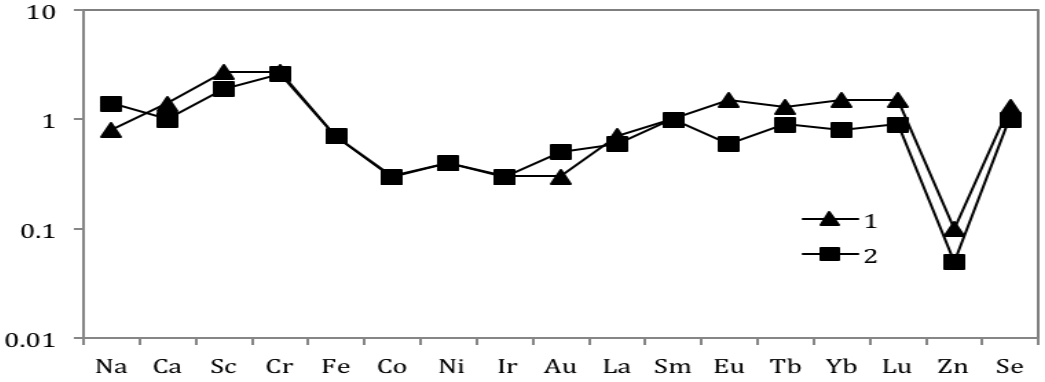

Fig. 3. Normalized to CI chondrite element contents in "coarse-grained" non-magnetic fractions from Atlanta enstatite chondrite. 1 - (160<d <260 μm); 2 - (260<d<360 μm).

The fine-grained non-magnetic fraction is enriched in lithophile - Sc, Cr, La, Sm, Eu, Tb, Yb, Lu and depleted in siderophile - Ni, Co, Au, Ir – elements. A characteristic feature of the distribution of trace elements in this fraction is the increased content of both light (1.5 x CI) and heavy (2.0 x CI) rare earth elements with positive Eu anomalies. The enrichment of fine-grained REE fractions with positive Eu-anomalies is possibly due to the fact that they contain the accessory mineral plagioclase, which is a concentrator of many rare elements. Only in the fine-grained fraction is there a strong fractionation between siderophile elements - the abundance of Au and Ir is an order of magnitude lower than that for Ni and Co. In the fine-grained fraction, a typical igneous distribution pattern of siderophile elements is observed with Ir depleted in comparison with Ni, Co, and Au. Such a distribution of siderophile elements can only be explained by evaporation and recondensation of fine-grained metal particles in the matrix material. This fraction differs from other size fractions in higher REE content, which may also be associated with evaporation processes matrix material. This fraction differs from other size fractions in the increased content of REE, which can also be associated with the processes of evaporation and recondensation of fine-grained silicate particles in the matrix substance as a result of impact processes. The volatile element Se (2.9 x CI) shows a distinct tendency to concentrate in the fine grained fraction, which indicates the interaction of this fraction with the gas phase at a relatively low temperature. Medium-grained (45 <d< 71 μm; 71 <d < 100 μm; 100<d<160 μm), and coarse-grained (160<d<260 μm; 260<d<360 μm) non-magnetic fractions (Fig. 2, 3) are depleted in light La (0.6 – 0.8 x CI) and enriched in heavy Lu (1.0 – 1.5 x CI) rare earth elements and have positive Eu anomalies: $(Eu/Sm)_{fraction}$ / $(Eu/Sm)_{CI}$ = 1.0 - 1.5. At the same time, Eu anomalies, as well as depletion in light REE, cannot be explained by nebular condensation. It is possible that positive Eu-anomalies in particle-size fractions are associated with plagioclase, since oldhamite is absent in the meteorite. The same abundances (0.2 x CI) for the "normal" siderophile elements Ni, Co, Au and refractory Ir are observed in all medium-grained fractions, indicating the absence of fractionation between siderophile elements, which

is typical for particles that have not undergone fractional crystallization. Such a prevalence of siderophile elements indicates the primacy of the composition of the metal included in the silicates of these fractions. In all medium-grained fractions, depletion of the volatile element Se (0.4 – 0.5 x CI) is observed, which indicates the absence of interaction of these fractions with the gas phase.

In coarse-grained fractions, in contrast to other fractions, when fractionating REE towards enrichment in heavy rare earth elements, both positive and negative Eu anomalies are observed. In these nonmagnetic fractions, the abundances of Ni relative to Co, Au, Ir, and CI chondrites are higher than the cosmic value, while in magnetic fractions, they are lower than the cosmic value. Such fractionation of siderophile elements is probably associated with metal sulfirization. The coarse-grained fractions are enriched in Se (1.0 – 1.3 x CI), but to a much lesser extent than the fine-grained fraction (2.9 x CI). REE fractionation towards enrichment in heavy rare earth elements is manifested in all non-magnetic fractions of the Atlanta chondrite - $(Lu/La)_{Atlanta}/(Lu/La)_{CI}$ = 1.2 – 2.2. This is obviously due to the fact that enstatite dominates in the meteorite, in which similar REE distribution spectra are observed. Except for the largest fraction, in all other size fractions of the meteorite, the REE distribution spectra have positive Eu anomalies – $(Eu/Sm)_{Atlanta}/(Eu/Sm)_{CI}$ = 1.0 – 1.5. In all magnetic fractions of the Atlanta chondrite, REE fractionation is manifested towards enrichment in heavy rare earth elements (Table 2). The ratios $(Lu/La)_{Atlanta}/(Lu/La)_{CI}$ = 1.5–4.0 are approximately 2 times higher than in the nonmagnetic fraction, which is obviously due to the presence of silicate inclusions in the metal in the form of one enstatite without accessory plagioclase.

In non-magnetic fractions, variations in the ratios $(Ni/Co)_{Atlanta}$ $/(Ni/Co)_{CI}$ =1.0 – 1.5; $(Ni/Au)_{Atlanta}$ $/(Ni/Au)_{CI}$ = 0.8 – 6.0; $(Ni/Ir)_{Atlanta}$ $/(Ni/Ir)_{CI}$ = 1.0 – 7.5 indicate the presence of both metal particles that have not undergone fractional crystallization (the ratio between siderophile elements is close to the cosmic one - medium-grained fractions) and particles with strong fractionation of siderophilic elements - fine-grained and coarse-grained fractions. In magnetic fractions, variations in the ratios $(Ni/Co)_{Atlanta}$ $/(Ni/Co)_{CI}$ = 0.6 – 2.10; $(Ni/Au)_{Atlanta}$ $/(Ni/Au)_{CI}$ = 0.2 – 2.2; $(Ni/Ir)_{Atlanta}$ $/(Ni/Ir)_{CI}$ = 1.0 – 7.5 show that the composition of the metal differs from that in nonmagnetic fractions in terms of Co and Au content. Such a distribution of siderophile elements in size fractions suggests that the material of the Atlanta meteorite underwent partial remelting due to impact processes. In the medium-grained non-magnetic fractions, the abundances of refractory Ir relative to the medium-volatile Au and CI of chondrites are equal to the cosmic one, and in the fine-grained and coarse-grained fractions they vary within (0.6 – 1.0 x CI). This indicates the presence in the silicates of metal particles that have not undergone fractional crystallization. In all magnetic fractions, the ratios of Ir to Au are less than the cosmic ones - $(Ir/Au)_{Atlanta}$ $/(Ir/Au)_{CI}$ = 0.58 – 0.76, which indicates the fractionation of these elements in the last fractions, possibly as a result of metal remelting due to impact processes. The coexistence of fractions with different elemental variations in the Atlanta chondrite is consistent with the model of impact fracture of the primary parent body of enstatite meteorites (Okada et al., 1988). The study of the distribution of trace elements in size fractions from the Atlanta enstatite meteorite showed that their distribution was affected by the agglomeration nature of the chondrite parent bodies, as well as the processes that led to structural changes in the meteorite.

Tab. 1. Contents of trace elements in non-magnetic fractions isolated from enstatite chondrite Atlanta, normalized to CI-chondrites.

Factions (μm)	Na	Ca	Sc	Cr	Fe	Co	Ni	Zn	Se	La	Sm	Eu	Tb	Yb	Lu	Ir	Au
1<d<45	0.7	0.7	1.7	6.3	1.4	0.2	0.3	0.03	2.9	1.5	1.8	2.0	2.1	2.2	2.0	0.04	0.05
45<d<71	0.8	1.0	2.3	1.9	0.5	0.2	0.2	<0.02	0.5	0.6	0.9	0.9	1.0	0.9	1.1	0.2	0.2
71<d<100	0.8	0.8	2.6	1.0	0.3	0.2	0.2	<0.02	0.4	0.8	1.0	0.9	0.9	0.9	1.0	0.2	0.2
100<d<160	0.9	1.8	2.4	1.2	0.3	0.2	0.2	0.03	0.5	0.6	0.7	0.7	0.9	1.2	1.3	0.2	0.2
160<d<260	0.8	1.4	2.7	2.7	0.7	0.3	0.4	0.1	1.3	0.7	1.0	1.5	1.3	1.5	1.5	0.3	0.3
260<d<360	1.4	1.0	1.9	2.6	0.7	0.3	0.4	0.05	1.0	0.6	1.0	0.6	0.9	0.08	0.9	0.3	0.5
enstatite	0.6	0.2	2.4	0.06	0.05	0.1	<0.02	<0.5	0.07	<0.2	<0.6	<0.7	<0.8	0.7	<0.02	<0.02	<0.02

Tab. 2. Contents of trace elements in magnetic fractions isolated from Atlanta enstatite chondrite, normalized to CI-chondrites.

Factions (μm)	Na	Ca	Sc	Cr	Fe	Co	Ni	Zn	Se	La	Sm	Eu	Tb	Yb	Lu	Ir	Au
1<d<45	0.1	0.2	0.09	0.1	2.3	2.9	6.1	<0.03	<0.3	<0.4	0.5	<0.6	<0.8	1.5	<1.0	1.9	2.8
45<d<71	0.04	<0.2	0.002	0.1	4.3	5.8	6.6	0.1	<0.3	<0.3	0.3	<0.4	<0.8	0.8	<1.2	4.8	8.1
71<d<100	0.06	0.3	0.06	0.06	4.6	7.0	6.7	0.08	<0.1	0.5	0.5	0.3	0.6	0.8	0.7	6.0	10.0
100<d<160	0.07	0.3	0.1	0.05	4.2	6.3	4.8	0.06	<0.05	0.2	0.2	0.4	<0.8	<0.6	<0.7	4.8	7.9
160<d<260	0.09	0.6	0.3	0.1	3.8	5.8	4.6	0.1	0.08	0.3	0.2	<0.2	<0.8	0.6	1.2	4.4	5.8
260<d<360	0.8	0.8	1.2	0.6	2.8	4.3	3.5	<0.2	<0.5	<0.8	<0.7	0.9	<0.8	1.0	1.2	3.0	5.2

Conclusion. Based on the features of the distribution of siderophile and rare earth elements in the size fractions of the Atlanta EL6 enstatite chondrite, it was assumed that the meteorite material was subjected to partial remelting due to impact processes, which also caused brecciation. It is assumed that these features of the distribution of elements were acquired as a result of the crystallization of impact melts. The origin of such melts could be as a result of impact melting in situ or impact melt ejections.

References

Baedecker P.A. and Wasson J.T. Elemental fractionations among enstatite chondrites *Geochim. Cosmochim. Acta*, 1975. 38, pp.735 - 765.

Kallemeyn G.W., Wasson J.T.. Compositions of enstatite (EH3, EH4,5 and EL6) chondrites: implications regarding their formation. *Geochim. Cosmochim. Acta.* 1986. V.50. P. 2153 – 2164.

Kolesov G. M., Shubina N.V., Lyul A.Yu.. Optimizing instrumental neutron activation analysis of extraterrestrial materials: fragments of lunar rocks, meteorites, chondrules and ultrarefractory inclusions. J. Anal. Chem. 2001. V.56. P. 1022 – 1028.

Okada A., Keil K., Taylor G. T., Newsom H.. Igneous history of the aubrite parent asteroid: evidence from Norton County enstatite achondrite. *Meteoritics,* 1988. 23, pp. 59 – 74.

Petaev M. I. and Skripnik A. Ya.. On the mineral composition of enstatite meteorites. Meteoretics, 1983. Vol. 42, p.86 – 92.

Sears D.W.. Formation of E chondrites and aubrites - thermodynamic model. *Jcarus* 1980. 43, pp.184-202.

Shukolyukov A., Lungmair G.W. (1998) The ^{53}Mn - ^{53}Cr isotope system in the Indarch EH4 chondrite: a further argument for ^{53}Mn heterogeneity in the early solar system. *Lunar Planet. Sci. Conf. XXIX*. # 1208.

Weisberg M. K., Ebel D. S., Connolby Ir., Kita N. T., Ushikubo T. (2009) Petrologic – geochemical study of chondrules in enstatite chondrites. *Lunar Planet. Sci. Conf.* XL2009. # 1886.

Lukanin O.A., Zharkova E.V. Redox regime during the formation of impact glasses.

Vernadsky Institute of Geochemistry and Analytical Chemistry, Russian Academy of Sciences
lukanin@geokhu.ru; zharkova@geokhi.ru

Abstract. The data obtained by the authors on the measurement of the intrinsic oxygen fugacity (fO_2) of glasses of impact origin at temperatures of 800–1100°C and 1 atm, using the method of solid electrolytic cells, are summarized. The objects of study were samples of various types of tektites from the European (Moldavite) and Australo-Asiatic (Indochinites, Philippinites, Australites) scatter fields, as well as melt impactites from two impact craters Zhamanshin (Kazakhstan) and Elgygytgyn (Russia). The determinations of fO_2 for glasses from the Libyan desert (LDG) are given for the first time. Comparison with fO_2 for volcanic glasses and rocks of various compositions demonstrates a significantly more reduced nature of tektite and, to a lesser extent, impactite glasses, which correlates with lower $Fe^{3+}/\Sigma Fe$ ratios in them. At the same time, the reduction processes during the formation of the bulk of the impact melts, obviously, were not accompanied by the reduction of iron to a zero-valent state and the formation of a metallic phase. The presence of mineral phases in impact glasses containing various forms of iron (metallic iron with an admixture of Ni, as well as wuestite, magnetite, hematite, etc.) is apparently associated with the non-equilibrium of the processes occurring at different stages of the formation of impact melts.

Keywords: intrinsic oxygen fugacity, tektites, melt impactites, Libyan Desert glass, impact craters, Elgygytgyn, Zhamanshin, impact events.

Introduction. The formation of impact glasses (tektites, melted impactites), which is accompanied by reduction reactions of oxide iron ($Fe^{3+} \rightarrow Fe^{2+}$ + (Fe^{o} ?), is one of the manifestations of the chemical transformation of the near-surface substance of planets as a result of high-velocity high-power impact events (Bazilevsky et al. 1983; Fudali , 1987; Feldman, 1990; Dressler and Reimold, 2001; etc.). Impact glasses, especially tektites, have significantly lower $Fe^{3+}/\Sigma Fe$ ratios compared to their original target rocks of different composition and genesis.

The first electrochemical determinations of the intrinsic oxygen fugacity (fO_2) for a number of tektite glasses confirmed the reducing conditions for their formation (Walter and Doan, 1969; Brett and Sato, 1984; Kadik et al., 2003). Various causes and mechanisms of Fe^{3+} reduction in the impact process are considered (Fudali, 1987; Engelhardt et al., 1987; Yakovlev et al., 1992; etc.). In particular, it is assumed that the main reason is redox reactions involving iron, which occur with a change in T, P, and fO_2 during melting and evaporation of the target substance as a result of impact (Lukanin and Kadik, 2007).

For a deeper understanding of the redox conditions for the formation of impact melts, we carried out electrochemical measurements of the intrinsic oxygen fugacity (fO_2) for glasses of various types of tektites from the European and Australo-Asian scatter fields, and also melt impactites from two large impact craters Zhamanshin (Kazakhstan) and Elgygytgyn (Russia) (Zharkova et al., 2020, Lukanin, Zharkova, 2021). This communication additionally presents the first results of the electrochemical determination of fO_2 in glasses from the Libyan Desert (LDG).

The main aims of this work are: 1) to find out, based on the generalization of all the data obtained, the dependence of fO_2 of impact glasses on their type, variety, and also on the degree of their remoteness from the parent crater; 2) to compare the redox state of tektites and melted impactites with the target rocks, terrestrial magmatites and meteoritic matter - chondrites.

Samples. The object of study was the following types of tektites: 1) moldavites (4 samples) from various places in Europe (Czech, Moravia), the formation of which is apparently associated with the release of superheated matter from the Ries impact crater in southern Germany (Engelhardt et al., 1987, etc); 2) indochinites from Indochina (sample 4), and 3) one sample from the Philippines and Australia, which, together with indochinites, belong to the extensive Australo-Asiatic scattering field and are genetically related to one giant impact event near the Indochina Peninsula (Folco et al., 2016). Among the indochinites, one specimen belongs to the Muong Nong type tektites, the other three have splatforms. Philippinite and australite are splash-form varieties. The chemical compositions of the used tektite glasses are given in (Lukanin and Zharkova, 2021).

Glasses of melt impactites were represented by samples from two impact craters: 1) from the Zhamanshin crater (Kazakhstan) - zhamanshinites (2 samples, impact bombs 20–25 cm in size) and tektite-like irghizites (2 samples, tubular glasses 1–3 cm in size); 2) from the Elgygytgyn crater (Chukotka) - 4 samples of impact bombs ranging in size from 2 cm to 3 m). The chemical compositions of impactite glasses used in experiments are given in (Zharkova et al., 2020).

The Libyan Desert glass sample (LDG), consisting of more than 98 wt. % SiO_2 (table), is typical of this type of impact glass, which was formed due to the melting of sandy rocks. The parent crater for them is not precisely established. According to a number of features, some researchers classify LDG not as impactites, but as Muong Nong type tektites (Barrat et al., 1997).

Table. Chemical composition of a glass sample from the Libyan Desert**.**

SiO_2	TiO_2	Al_2O_3	FeO*	MgO	CaO	Na_2O	K_2O	MnO	Total
96.96	0.22	0.60	0.14	0.02	0.01	0.02	0.03	0.02	98.02

Notes. Average values measured on Cameca SX-100 at 5 points. FeO* - total content of iron in the form of FeO.

Method. For experimental studies, small pieces of clean transparent glasses (1-3 mm) with a total weight of 70-90 mg were used, carefully selected under a binocular in order to avoid the presence of weathering crusts, bubbles, as well as crystalline and other inclusions. The determinations of fO_2 of glasses were carried out on a high-temperature furnace with two solid zirconium electrolytes at 1 atm in the temperature range from 800°C to 1050-1100°C with a cyclic increase and decrease in temperature with a step of 30-50°C during heating and cooling of each sample (for more details, see in Ariskin et al., 2017). The exposure time at each temperature to obtain the equilibrium value of fO_2 was 40–60 min. Measurement accuracy fO_2 ±0.1-0.2 log. units.

Results and discussion. For all studied glass samples, with the exception of LDG, the log fO_2 values measured at a given temperature during its rise and subsequent decrease (7-10 measurements in the range of 800-1050°C) remained constant within the measurement error, forming a clear linear dependence log $fO_2 = A - B/T,K$ (where A and B are constants) with a correlation coefficient higher than 0.98.

On Fig.1 shows examples of log fO_2 values for tektite glasses from different scatter fields. All of them in the studied temperature range are located

between the buffer equilibria IW and WM. At T > 900-950˚C, the lowest fO_2 are characteristic of moldavites. For indochinites, among which there are more diverse types of tektites (Muong Nong type, splat forms, etc.) and which are located much closer to the parent impact crater than philippinites and australites, wider variations in fO_2 are observed.

The log fO_2 values for glasses from Elgygytgyn and Zhamanshin melted impactites are comparable with some types of indochinites, but somewhat higher than those for moldavites. On the log fO_2 - 10^4/T,K diagram, they are generally located in the same fO_2 region between IW and WM (Fig. 2). For the impact bomb glasses of the Elgygytgyn crater, there is no correlation between the position of the lines in the diagram depending on the composition and size of the bombs. Note the sharp difference in fO_2 values for glasses from tektite-like irghizites from the Zhamanshin crater compared to tektites and melt impactites. The temperature dependence lines of log fO_2 for irghizites have a noticeably steeper slope than the corresponding lines for tektites (Fig. 1) and melt impactites (Fig. 2). At elevated temperatures (≥1040°C) fO_2 of irghizites reaches the values of the QFM buffer.

.

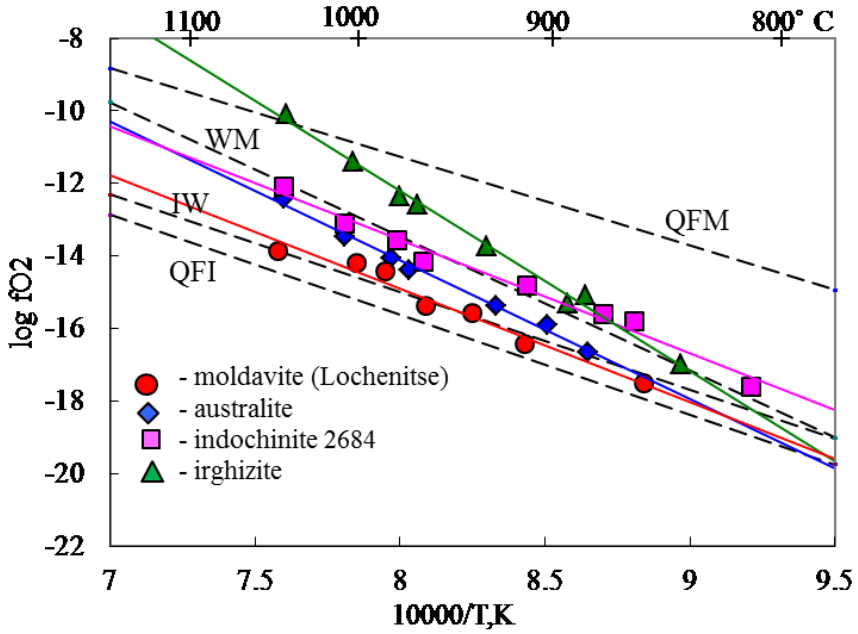

Fig. 1. Dependence of log fO2 – 104/T,K for glasses of various types of tektites and irghizite.

Dashed lines are buffer equilibria: IW - iron-wustite, WM - wustite-magnetite, QFI - quartz-fayalite-iron, QFM - quartz-fayalite-magnetite.

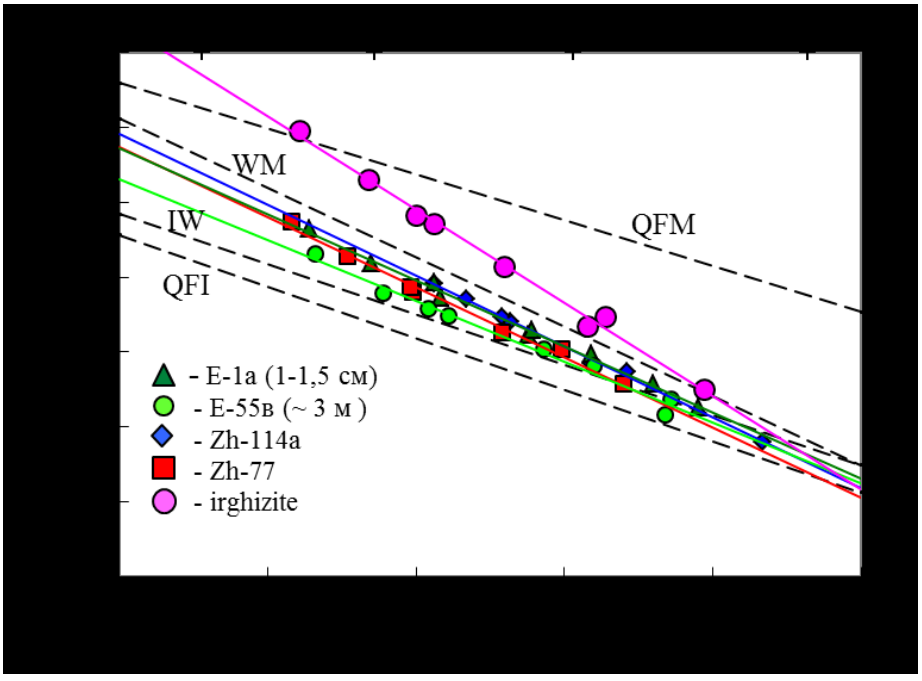

Fig. 2. Dependence of log fO_2 – 10^4/T,K for glasses of melt impactites from Elgygytgyn crater (samples E-1a, E-55b) and Zhamanshin crater (Zh-114a, Zh-77, irghizite).

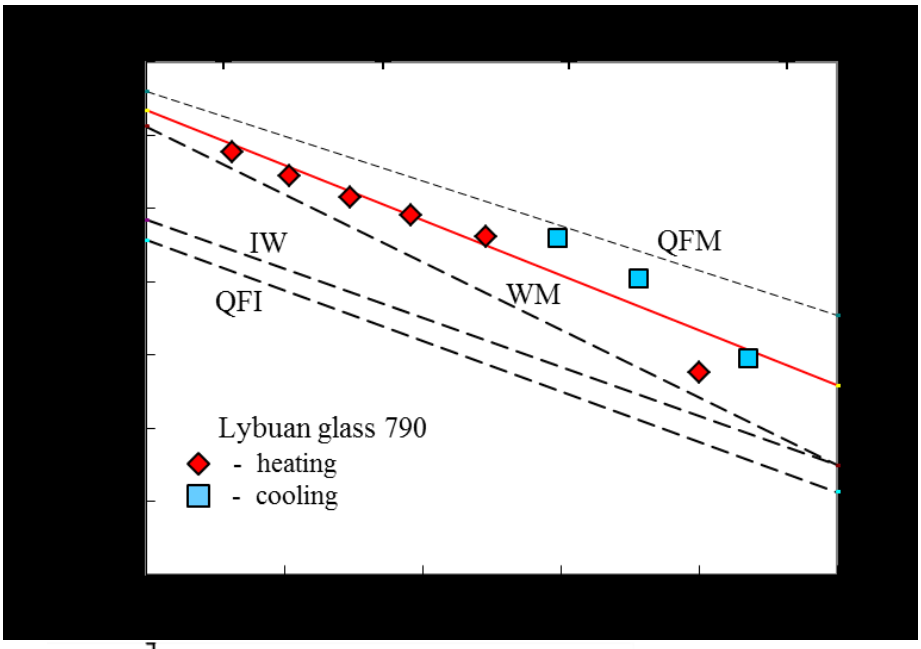

Fig.3. Log fO_2 values measured for glasses from the Libyan Desert with an increase and decrease in temperature. The solid line is the log $fO_2 - 10^4/T,K$ dependence for all the data obtained.

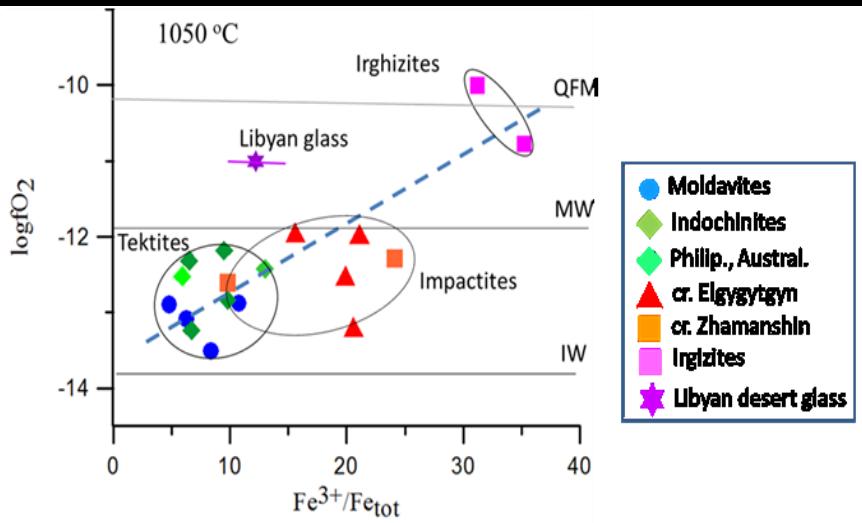

Fig. 4. Log fO_2 ratio at 1050°C and Fe^{2+}/Fe_{tot} in tektites and melted impactites.

Experiments with glasses from the Libyan Desert have shown that the log fO_2 values measured with decreasing temperature are significantly different (upward) from those values that would be expected based on the temperature dependence based on data obtained with increasing temperature (Fig. 3). One possible reason is the release of water when the sample is heated. The content of H_2O in LDG is one of the highest among other impact glasses (0.120 ± 0.045 wt.%), while in glasses of tektites, including indochinites of the Muong Nong type, it is 0.010 - 0.016 wt.%, and in glasses of impactites , including irghizites, does not exceed 0.051 wt % (Beran and Koeberl, 1997; Kadik et al. 2003).

In general, the fO_2 values obtained for LDG significantly exceed the fO_2 values for the WM buffer and for all the studied glasses of impact origin, with the exception of irghizites. This gives grounds to believe that the formation of melts (glasses) of LDG and irghizites occurred under much more oxidizing conditions. Perhaps, as some authors suggest, as a result of the fall and explosion of comets (Wasson, 2017; Gornostaeva et al., 2018).

It should be noted that the measured fO_2 of glasses from tektites and impactites of the Elgygytgyn and Zhamanshin craters and the $Fe^{3+}/\Sigma Fe$ ratios determined in the same samples by Mössbauer spectroscopy (Rusakov et al. 2007, Volovetsky, 2010) demonstrate a relatively well-pronounced correlation: the less $Fe^{3+}/\Sigma Fe$ in glasses, the lower fO_2 (Fig. 4).

Conclusion. The redox state of impact melts (glasses) is determined by many factors. It is assumed that the most important reduction factor is the temperature of the substance involved in the impact process, which is determined by the impact power. In addition, obviously, the initial composition and redox state of the target rocks, as well as the impactor itself, are of significant importance. A diverse combination of these factors can explain the observed variations in fO_2 during the formation of impact melts (glasses).

All available experimental determinations of fO_2 for glasses of tektites and impactites, with the exception of irghizites and LDG, in a wide range of temperatures are significantly lower by 1–3 orders of fO_2, which are characteristic of igneous melts (glasses) of crustal and mantle origin. Lower $fO_2 \leq fO_2$(IW) were obtained by the electrochemical method for the meteorite material of chondrites, which, in addition to silicate phases, contain Ni-iron and troilite (Walter and Doan, 1969; Brett and Sato, 1984; Osadchii et al., 2017). At temperatures above the full melting temperature ($\geq$ 1000–1050°C), fO_2 for all impact glasses studied is 0.5–2 log units higher than fO_2(IW), i.e. significantly higher than those values of fO_2 that correspond to the equilibrium of the metallic phase of iron with the silicate melt.

Thus, the reduction processes during the formation of the bulk of the impact melts, obviously, were not accompanied by the reduction of iron to a zero-valent state and the formation of a metallic phase. At the same time, metallic Fe (with an admixture of Ni) as well as wustite, magnetite, hematite, and other phases were found in tektites and impactites in the form of micro- and submicroscopic inclusions (Brett, 1967; Feldman, 1990; Mineeva et al., 1984; Vishnevsky and Raitala, 2003, etc.). The presence of phases containing iron of different valence forms in impact glasses is apparently associated with the nonequilibrium of the processes that occur at different stages of the formation of impact melts (glasses): (a) during melting and evaporation of the initial target material and meteorite striker; (b) subsequent cooling of the melt-vapor mixture; and, finally, (c) during the quenching of melts during a catastrophic increase in the volume of the explosive cloud and the ejection of material outside the impact crater.

The work was carried out according to the state order of GEOKHI RAS

References

Ariskin A.A., Fomin I.S., Zharkova E.V., Nikolaev G.S. Redox regime of formation of ultramafic and gabbroids of the Yoko-Dovyren massif (according to the results of measurements of the intrinsic oxygen fugacity in olivine) // Geochemistry International. 2017. V. 55, No 7, P. 595- 607.

Barrat J. A., Jans B.M., Ammossé J., Rocchia R., keller F., Poupeau G.R., Diemer E. Geochemistry and origin of Liyan Desert glasses // Geochim. Cosmochim. Acta. 1997. V.61. P. 1953-1959.

Bazilevsky A.T., Ivanov B.A., Florensky K.P. etc. Impact craters on the Moon and planets. M.: Nauka, 1983, 226 p.

Brett R. and Sato M. Intrinsic oxygen fugacity measurements on seven chondrites, a pallasite, and a tektite and redox state of meteorite parent bodies.// Geochim. Cosmochim. Acta. 1984. V. 48. P. 111-120.

Dressler B.D., Reimold W.U. Terrestrial impact rocks and glasses. // Earth-Science Reviews. 2001. V. 56. No 1-4. P. 205-284.

Engelhardt W.V., Luft E., Arndt J., Schock H., Weiskirchner W. Origin of moldavites. // Geochim. Cosmochim. Acta. 1987. V. 51. P. 1425-1443.

Feldman V.I. Petrology of impactites. 1990. M.: Publishing House of Moscow State University. 299p.

Folco L, D'Orazio M, Gemelli M, Rochette P. Stretching out the Australasian microtektite strewn field in Victoria Land Transantarctic Mountains // Polar Science. 2016. V. 10. P.147-159

Fudali R.F., Dyar M.D., Griscom D.L., Schreiber H.D. The oxidation state of iron in tektite glass. // Geochim. Cosmochim. Acta. 1987. V. 51. P. 2749-2756.

Gornostaeva T.A., Mokhov A.V., Kartashov P.M., Bogatikov O.A. Type of impactor that formed the crater Zhamanshin (Kazakhstan) // Petrology. 2018, Vol. 26, No. 1, pp. 82–95.

Kadik A.A., Lukanin O.A., Zharkova E.V., Feldman V.I. Regime of oxygen and hydrogen (water) during the formation of tektites. // Geochemistry International. 2003. Vol. 41. No. 9. P. 865- 880.

Lukanin OA, Kadik AA Decompression mechanism of iron oxide reduction in tektite melts during their formation in the impact process. // Geochemistry International. 2007. V.45. No. 9. P. 857-881.

Lukanin O.A., Zharkova E.V., Senin V.G. Redox state of tektites from different stray fields according to electrochemical determinations of oxygen intrinsic fugacity. // Doklady Earth Sciences, 2021, Vol. 497, Part 2. P. 295–299.

Mineeva R.M., Bershov L.V., Marfunin A.S., Feldman V.I., Speransky A.V. Structural forms of iron and manganese in tektites and impactites according to EPR data. // Mineral. Magazine. 1984. V. 6. No 2. P. 30-35.

Osadchii V.O., Fedkin M.V., Osadchii E.G. Determination of the equilibrium fO_2 in bulk samples of H, L, and LL ordinary chondrites by solid-state electrochemistry. // Meteoritics and Planetary Science. 2017. V. 52. No 10. P. 2275-2283.

Rusakov V.S., Volovetsky M.V., Lukanin O.A. Mössbauer studies of glasses of impact and volcanic origin. // West. Moscow University. Physics. 2007. No 3. P. 57-62.

Vishnevsky S.A., Raitala J. Native iron, wustite and magnetite in impactites of Janisjarvi and Grandos Craters (The Baltic shield) // 66th Annual Meteoritical Society Meeting, 2003. #5072.

Volovetsky M.V. Valence and structural state of iron atoms in glasses of impact and volcanic origin. Diss. for the competition cand. chem. Sciences. Moscow, GEOKHI, 2010, 128 p.

Walter L.S., Doan A.S. 1969. Determination of the P_{O2}-T equilibrium of indishinite tektite (abst.) //NASA Astrophysics Data System (ADS). Meteoritical Society. V.4. P. 295-296.

Wasson J.T. A thermal-plume origin of layered and splash-form tektites and Libyan Desert glass //Lunar and Planetary Science XLVIII. 2017, 2916.pdf

Yakovlev O.I., Dikov Yu.P., Gerasimov M.V. 1992. Problems of oxidation and reduction in the impact process. // Geochemistry. 1992. No 12. P. 1359 - 1370.

Zharkova E.V., Lukanin O.A., Tsekhonya T.I., Senin V.G. 2020. Determination of the redox state of impactites from the Elgygytgyn and Zhamanshin impact craters by the electrochemical method. Proceedings of VESMPG-2020. Moscow, 2010. P. 234-238. http://www.geokhi.ru/DocLab17/RASEMPG-2020.pdf

Tselmovich V.A.[1], Maxe L.P.[2] Microstructure and composition of magnetic microspheres anthropogenic and cosmogenic origin. UDC: 628.511

[1] Borok Geophysical Observatory, the Branch of Schmidt Institute of Physics of the Earth, Russian Academy of Sciences, Borok, Yaroslavl region, 152742 Russia tselm@mail.ru, ksasha@borok.yar.ru tel. +7(9066327448)

[2] Belarusian State Universisty of Food and Chemical Technologies. Mogilev region, 3, Shmidt Avenue, Mogilev, 212027 Belarus larissa_maxe@rambler.ru tel. +375298428209

Abstract. Samples of Mt-microspheres of various origins, including those obtained in industrial processes, have been studied. The authors concluded that the morphological characteristic of Mt-microspheres only, without of consideration of synthesis processes, are not sufficient to diagnose their origin. The authors revealed a distinctive feature of Mt-microspheres and other microparticles that were extracted from sedimentary rocks and considered as cosmogenic, it is the presence of morphology and shapes characteristic for by-products of metal processing and target products of plasma chemical synthesis.

Keywords: Mt-microspheres, morphology, cosmogenic, plasma chemical synthesis.

Introduction. Microspheres are one of the most informative and widespread types of microscopic inclusions that are found in the composition of environmental objects, the atmosphere, hydrosphere and lithosphere. Magnetite magnetic microspheres (Mt-microspheres), which are formed in a variety of processes, both natural and industrial, have much in common in the structure and morphology. In search of differences between Mt-microspheres of various origins, many scientists have studied the characteristics of the composition, structure, and morphology to identify features and criteria for classifying them as cosmogenic, volcanic (geotectonic), or technogenic, more generally, anthropogenic. We have considered Mt microspheres in connection with the processes in which they are formed as the final products of the ultrafast oxidation reaction. With regard to morphology, we proceeded from the principle: common or similar morphological characteristics indicate not specifically the origin, but the similarity of the physical conditions and physicochemical processes of their structure formation. Taking this into account, the morphological features of Mt-microspheres only are not sufficient for diagnosing their origin, since the types of crystal structures and morphology, as their macro manifestation, are subject to physical laws that are realized under specific conditions and processes. Images of Mt-microspheres obtained using scanning electron microscopy (SEM) indicate the characteristic morphological manifestations of the crystal structure of magnetite: dendritic, block, stellate, ablative.

Materials and methods. Natural Mt-microspheres are formed in tectonic processes and in atmospheric ones: during ablation and explosions of meteoroids, precipitation of dispersed flows of cosmic dust, cometary matter. Anthropogenic Mt-microspheres are products of human activity, ancient and modern. The source of heating of melts erupted by volcanoes is the endogenous heat of the Earth, and the outburst of lava flows - melts occurs due to very fast physical and chemical processes, which often have an explosive character. At the same time, almost all types of volcanic eruptions occur accompanied by atmospheric electricity – lightning, generating plasma flows (Sandimirova et al., 2009). Meteoroids entering the Earth's atmosphere at high and ultra-high-hypersonic speeds are subject to kinetic heating, experiencing aerodynamic resistance. At present, the most commonly used model to describe the motion of a meteoroid in the atmosphere is based on the consideration of two stages. The stage of sharp unsteady deceleration leads to ablation of the body due to melting and evaporation. The final stage of kinetic overheating of a meteoroid proceeds as an explosive and is accompanied by the loss of its mass due to crushing, ejection of fragments, melt, vapors and plasma. Fragments become further links in the sequence with deceleration and final explosion (Egorova et al., 2016).

The current state of industrial production and communications creates and supply into the environment a huge flow of microparticles, including Mt-microspheres. Technological processes in metallurgy and metalworking, the fuel and energy sector are often accompanied by the formation of waste in the form of Mt-microspheres. Machine tools and tools for the processing of iron and its alloys (cutting, turning, abrasive processing), friction and electrical contact units are sources of the formation of the smallest drops of melts. Microdrops of melts, iron vapor and plasma are formed during the operation of equipment for welding and cutting metal (gas-flame, electric arc, plasma), in metallurgical processes. Plasma works in plasma-chemical

processes for obtaining metal powders, plasma sputtering and spraying. In materials science, based on the analysis of SEM images and composition data, it has been established that dendritic crystallization, characteristic of metals and alloys, is observed for many substances and materials, including magnetite. In this case, dendritic crystallization of melts with different compositions forms morphologically similar structures.

Taking into account this feature of crystallization, the authors set the analytical task to compare the morphology of Mt-microspheres extracted from various sources of accumulation of cosmic dust particles in sedimentary rocks (tripoli, peat, sand of the Kamil crater) with Mt-microspheres formed in technological processes that accompanying by the formation of melts, also of vapors and plasma containing iron. To detect Mt-microspheres in environmental objects, optical and USB microscopy was used; to obtain targeted scientific information and solve research problems, the authors used SEM (Tselmovich et al., 2021).

For a comparative analysis of Mt-microspheres, in accordance with the task, for the selection of technogenic samples, such industrial processes were selected in which there are stages of formation of the target or by-product in the form of melt, droplets, vapors and plasma. Metalworking – sharpening on an abrasive wheel, is accompanied by a loss of mass of the part in the form of hot microdroplets of the melt, oxidized in air. Electric current in the circuit of a moving electric transport – the sliding contact of the tram rode with pantograph periodically subjected to strong heating and becomes a source of melt microdroplets. Also one process is a heating to the melting temperature by electric arc welding, which is the source of plasma and dispersion of melt microdroplets. Heating to the melting temperature is also quickly achieved in the operation of industrial plasma torches. Metallurgical melting in a steelmaking converter proceeds with the release of vapors and melt microdroplets, which are oxidized and condense into Mt-microspheres. Samples of particles formed in these processes were taken in Mogilev, Belarus (sharpening – workshop "Sportmaster", electric welding – OOO "STRIM", cutting with a plasma torch – BRU), and in Magnitogorsk, Russia ("dust" was taken near the converter, micro drops were collecting under tram pantograph). The selected "production" samples were preliminarily studied using USB microscopy, the necessary objects were isolated and examined at the Borok Geophysical Observatory of the IPE RAS using a SEM Tescan Vega II.

Results and discussion. The results of the study of the morphology of Mt-microspheres extracted from samples of natural and technogenic origin, using SEM, were summarized in data base, part of the data in image format is presented in Figures 1 and 2. Magnetite dendritic structures and ablation there are in all natural Mt-microspheres compared using of the morphology characteristic; analogies are also manifested in the morphology of the inner part of hollow microspheres. Microspheres extracted from peat are distinguished by a variety of shapes and structures, Figures 1.

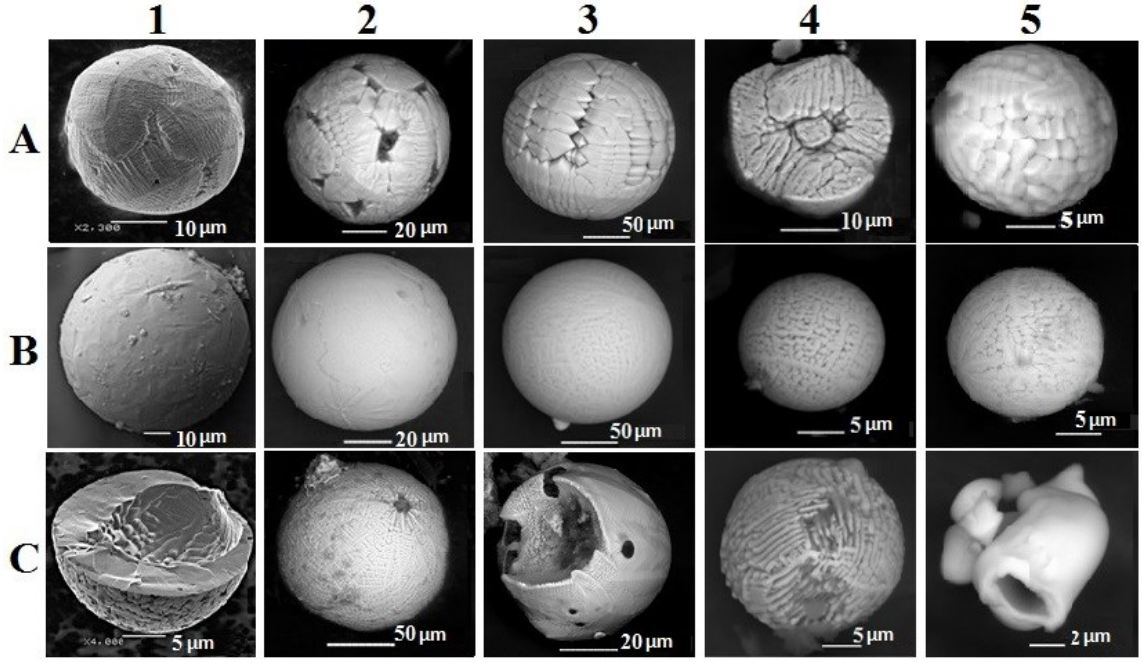

Fig. 1. Horizontal images of Mt-microspheres: A – dendritic, large-block; B – ablative, mesh; C – structures with ajar interior. Sources from which Mt-microspheres were isolated, vertically: 1 – desert sand from the Kamil crater, Egypt (Bignami et al., 2014); 2 – tripoli from the "Stalnoye" deposit, Khotimsk district, Mogilev region, Belarus; 3 – peat, Gonchanskoye deposit, Mogilev region, Belarus; 4 – tundra peat, Russia; 5 – peat, Myshkin, Yaroslavl region, Russia (with fine volcanic dust).

Metal particles formed during sharpening of steel blades with corundum abrasive, melt drops as sparks are ejected from the working area, oxidized to magnetite, forming a dendritic or block structure. Part of the melt, hitting the fence, cools and forms particles of irregular shape, but a significant part of the cut metal does not heat up to the melting temperature and is represented by particles of drain chips. Converter steel smelting is accompanied by the formation of Mt-microspheres with a dendritic, block, star-shaped structure; there are present microspheres with an orange-peel surface similar to an ablation one. For thin hollow microspheres characteristic is a difference between the morphology of the outer surface and inner walls, the crystallites of the surface of the microspheres and the cavity are connected by a non crystallized phase.

Coarsely dendritic hollow Mt-microspheres often have through grains of crystallites directed from the surface to the center, Figure 2.

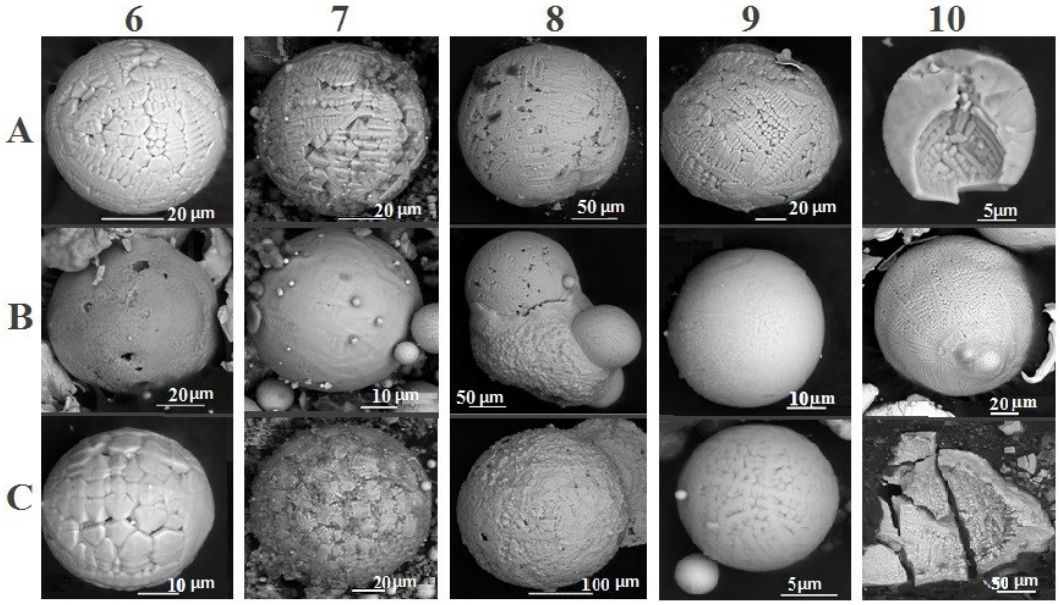

Fig. 2. Horizontal images of Mt-microspheres: A – dendritic; B – ablative, fine mesh; C – finely blocky, stellate, finely branched structures. Sources from which Mt microspheres were isolated, vertically: 6 – sharpening with a corundum abrasive wheel; 7 – converter melting of steel; 8 – plasma torch cutting iron-nickel alloy; 9 – electric arc cutting of metal; 10 – under pantograph of the tram.

When cutting an iron-nickel alloy (food-grade steel) with a plasma torch, irregularly shaped particles, dendritic Mt-microspheres, and cooled intermediate phases were formed as by-products. In the process of electric arc welding, dendritic Mt-microspheres with through crystallites and thin-walled hollow, brittle, as well as many non-spherical particles were formed as waste, Mt-microspheres with an ablation surface are rare. Mt-microspheres with a dendritic structure, hollow, also particles of mechanical destruction – drain and composite chips were sliced by electric contact of pantograph; ablative-type Mt-microspheres are rare.

Considering the Mt-microspheres as the end products of the reaction, we noted the general stages and nature of the high-temperature chemical reaction. In the form of microdrops from the phase of the metal melt, which is subjected to ultrafast oxidation by atmospheric oxygen, solid-phase magnetite is almost instantly formed, which has a higher melting point. Cooling, magnetite crystallizes to form microspheres with dendritic, block, reticulate morphology, or an ablative orange-peel surface. Depending on the speed of removal from the source of the release (boiling, splashing or explosion) and the distribution of temperatures along the flight path, a “tail” of particles is formed, and when they settle on the surface, a trace of scattering is formed. The characteristics of microparticles of the trace of scattering (shape, morphology, material and elemental composition, and others) are a kind of information "projection" of the event. In the processes considered above, the formation of Mt-microspheres with ablation is a plasma-chemical reaction of iron oxidation (Katasonov et al., 2013). Spatially separately, simultaneously or sequentially, other plasma-chemical reactions and physical processes proceed with the formation of other forms of microparticles.

Studies have established that the synthesis of several forms of magnetite can occur in the plasma-chemical process, one of which ε-Fe_2O_3 is distinguished by a significant coercive force, strong absorption of microwave radiation, and chemical stability (Shanenkov, 2018). Owing to its special properties, the ε-Fe2O3 phase is distinguishable in a mixture of Mt-microspheres extracted from samples

of sedimentary rocks or a mass of magnetic impurities extracted from processed rocks.

Conclusions. The physicochemical processes of the formation of Mt-microspheres in natural processes, during the combustion and destruction of meteoroids, are in many respects similar to industrial processes that proceed with the formation of melts, vapors and plasma. Mt-microspheres and microparticles of other forms in sedimentary rocks, which are classified as cosmogenic, are similar in shape and morphology and are comparable with metalworking microparticles, with the target products of plasma chemistry. The morphological features of Mt-microspheres, isolated from the entire complex of characteristics of microobjects in the trace of their scattering, cannot serve as the only criterion for classifying them as cosmogenic in origin. The presence of microparticles in sedimentary rocks, similar in shape and morphology to particles that are formed in technological operations and plasma-chemical processes, allows us to set new tasks in order to conduct a comprehensive study of microparticles in the trail of scattering of a space event on the surface and in geological layers in comparison with the average background composition microparticles of cosmogenic origin.

The work was carried out within the framework of the state task of the IPE RAS

References

1. Bignami L., Guaita C., Pezzotta F., and Zilioli M. Micro-spherules near the Kamil crater. Mem. S.A.It. Suppl. Vol. 26, 25. 2014.
2. Glukhov M. S. Comparison of metal microspheres of cosmic and technogenic dust / M. S. Glukhov, R. Kh. Sungatullin, B. M. Galiullin // Minerals: structure, properties, research methods: materials of the IX All-Russian Youth Scientific Conference (Yekaterinburg, February 5-8, 2018). - Yekaterinburg: Institute of Geology and Geochemistry, Ural Branch of the Russian Academy of Sciences, 2018. P. 48 - 49.
2. Egorova L.A., Lokhin V.V. On the two-stage destruction of a meteoroid with a terminal flash // Vestn. Moscow university Ser. 1, Mathematics. Mechanics. 2016. No. 4. P. 43 – 48.
3. Katasonov P.A., Garifullin R.A., Pronin V.P. Structure and chemical composition of magnetite synthesized in the plasma-chemical process // Proceedings of the Russian State Pedagogical University. A.I. Herzen. 2013. No. 150. pp. 83 - 89.
4. Sandimirova E.I. Microspherules as indicators of fluid (fluid-magmatic) processes in areas of modern volcanism // Volcanism and geodynamics. IV All-Russian Symposium on Volcanology and Paleovolcanology. Petropavlovsk-Kamchatsky, 2009. P. 806 - 809.
5. Shanenkov I.I. Plasma-chemical synthesis of dispersed iron oxides with a high content of epsilon phase in a high-speed jet of electric discharge plasma: thesis of a candidate of technical sciences. FSBI "National Research Tomsk Polytechnic University". Tomsk. 2018. - 153 p.
6. Tselmovich V.A., Maxe L.P. On the Cosmogenic Nature of Microspheres from Tripoli and Desert Sands. // Proceedings of the XXII Intern. conference "Physical-chemical and petrophysical research in the geosciences", Moscow, September 27 - 29, Borok, October 1, 2021. Moscow, 2021. P.289 - 292.

Ustinova G.K. Basic processes of matter separation at the formation of planetary systems. UDC: 123.456

Institute of Geochemistry and Analytical Chemistry (GEOKHI) of RAS, Moscow ustinova@dubna.net.ru

Abstract. The energy income into the interstellar medium of our Galaxy due to supernova outbursts fills it homogeneously with the injected matter. The planet formation in the cosmic space implies, at least, the separation of cosmic matter by mass. The possible basic magneto-hydrodynamic processes (e.g., the diffusion acceleration of particles in shock waves, the motion of matter inside vortexes, the behavior of matter in shock events and the picture of motion in the mixed molten matters), which lead to such separation of the matter, are considered. Some possible impacts of the processes during the formation and evolution of the pallasites are discussed.

Keywords: supernova flares; magneto-hydrodynamic processes; gravitation; planet formation.

Up to nowadays, the problems of planet formation have not reached the final consistent solution (see, e.g., Markelova and Snytnikov, 2012). The approach based on the idea of formation of primary planets as a result of fusion of dust particles of molecular clouds into the larger and still larger particles, successively, and the creation of planetesimals (Weidenschilling, 1980; Weidenschilling and Cuzzi, 1993) seems to be the most realistic one. Such bodies, being already large enough, accumulate the surrounding dust constituent over a long time period and, colliding with each other, lead to the formation of planets of different types in the elastic and inelastic collisions (Pollack, 1984).

In so doing, the key question arises: where did the dust particles in molecular clouds emerge from ? One needs to assume that the primary conditions of formation of planetary systems included some magneto-hydrodynamic processes of matter separation by mass and the presence of gravitational centers retaining, in their surroundings, the local groups of generated bodies.

At present it is considered to be well-acknowledged that the main energy income into the interstellar medium of our Galaxy is provided by supernova outbursts (Berezinsky et al., 1990). The

discovery of the universal mechanism of cosmic ray acceleration in shock waves accompanying the supernova outbursts (Ellison and Eichler, 1984) served as a reliable justification of this hypothesis .

During the motion of the ejected supernova matter in the turbulent interstellar medium, a shock wave representing the magneto-hydrodynamic rupture is being formed, at the front of which – in the area of matter compression – the regular magnetic field suffers a jump and, besides, the stochastic magnetic field of plasmatic turbulence is developing, which creates the scattering centers for the diffusion scattering of charged particles. The physical meaning of the acceleration mechanism is in the fact that, as a result of the diffusion scattering, the charged particles may cross the compression region at the wave front for many times, acquiring the energy increase in the emerging induction electric fields, i.e. the longer is the period when the particles are retained in the wave front region – the stronger is their acceleration. In other words, the larger are the particle velocity and, hence, its path before scattering – the more frequent is the particle return to the front region with getting the increase of velocity, and the greater is the distance from which this particle may return. As a result, the power spectrum of particles by momentum is formed, which is equivalent, in the relativistic case, to the power energy spectrum $F(E) \sim E^{-\gamma}$ with the exponent $\gamma = (\sigma+2)/(\sigma-1)$, where σ is the degree of matter compression at the shock front. Analogously, the heavy ions with the large path will have the priority in acceleration, which leads to the enrichment of the spectrum with heavy ions proportionally to A/Z, where A is the mass number and Z is the ion charge. Thus, it is peculiar that at high particle energies ($\geq 10^{15}$-10^{17} eV) the spectrum consists of iron practically by ~100% (Haungs, 2009).

The pumping of particles from the low-energy region of spectrum to the high-energy one leads to the increase of fluxes of nuclear-active particles above the threshold energy of nuclear reactions and, respectively, to the increase of velocities of isotope formation in spallation reactions (Ustinova, 2013). Besides, the change of energy spectrum of nuclear-active particles leads to the change of mean-weighted (by spectrum) production cross sections of many isotopes, the excitation functions of which are sensitive to the shape of particle spectrum. As a result, in the reservoirs processed by shock waves – for example, in the expanding supernova shells – quite different ratios of isotopes and elements are formed, as compared with the matter not affected by such processing. Indeed, in the samples of extraterrestrial matter, multiple isotopic anomalies are observed, which might be conditioned by such violations of isotopic ratios (Ustinova, 2013).

Thus, just at the earliest stage of the Solar system formation, its matter was suffering the separation by mass due to the fact that, in the magneto-hydrodynamic processes of acceleration, namely the heavier particles acquired the greater velocities. Already at the stage of the most simple differentiation of this kind, under the rotation in the gravitational field of the Sun (the free downfall acceleration g = 274.1 m/sec^2) the stable layers of matter rotation (future orbits of celestial bodies of different size and density) are formed at different heliocentric distances. In each of these layers, in the conditions of magneto-hydrodynamic turbulence, the vortexes of different scale are being formed, which leads to the beginning of matter consolidation. The fact is that, during the motion inside the vortex, the matter separation proportionally to its mass ($\rho = m/V$, where ρ is the matter density, m is its mass and V is its volume) also takes place. In particular, at the Earth orbit (1 a.u.), with the free downfall acceleration equaling g =9.8 m/sec^2 , the bodies having the larger density reach the vertex of a vortex more quickly (Ustinova, 2006). This testifies to the fact that the processes of matter separation by mass represented one of the important factors of the formation and evolution of bodies of the Solar system since the earliest stage of its generation.

Possibly, such processes are evidenced by pallasites – the very rare type of iron-stony meteorites, which are peculiar for the visible implantation of olivine grains into the iron-nickel matrix. Up to nowadays, there is no consistent version of their origin. However, already in 1964, E. Anders supposed there formation in the transitional zone between the kernel and the mantia of the parent body (Anders, 1964). At present the concept of matter differentiation in the transitional zone, within the problem of the origin of pallasites, is accepted by many authors (Tarduno et al., 2012; Scott and Taylor, 1991, et al.).

The pallasite of Seimchan, found in the Magadan region in 1967, provokes the great interest and, besides, its separate fragments can be encountered up to now. It is peculiar for the shifts of olivine clusters with respect to the iron-nickel martix, observed in some places, so that the pictures made of vidmanshtetten lines, testifying to the metal crystallization in the cosmic space conditions over milliards of years – i.e. to the substantial age of this pallasite and to its formation at the earliest stage of the Solar system generation – become quite noticeable.

The presence of such shifts may indicate to a shock event in the history of the parent body of Seimchan (Hisina et al., 2020), the possibility of which is supposed also in the hypotheses of origin of other pallasites as well. It is natural that, in doing so,

the matter separation by mass arises again, but here its effect is opposite to the one for two previously considered processes: at the shock moment, the lightest particles gain the greatest velocities. The peculiarity of shock waves at cosmic velocities is represented by high temperatures and the melting of matter, which allows one to understand many of the observed effects in the pallasite of Seimchan – it is studied in detail in (Hisina et al., 2020). In particular, under the local shock melting, the rounding of the primarily angle-shaped and fragmentary olivine grains and the neighboring areas of the incorporating iron-nickel matrix takes place. One of the mechanisms of differentiation of such a mixed melted substance may be the different buoyancy of the components being mixed (Scott and Taylor, 1991), i.e. again we see the mass separation here : the lighter particles have the better buoyancy (the olivine density is ~3.4 g/cm^3 , whereas the iron density is ~7.8 g/cm^3). As a result of the available research, a possible non-contradictory scenario of the origin of the Seimchan pallasite at the collision of an iron meteorite with the upper layers of the olivine mantle of an asteroid appears.

The round olivine grains of pallasites represent a fine material for the search of traces (tracks) of heavy and superheavy nuclei in cosmic rays, which is connected with the problem of existence of the stability islands in the Periodic table of elements (Alexeev et al., 2019). The estimates of charge of three registered particles, being available in the first approximation, correspond to the range of $105 < Z < 130$, which is consistent with the expectations. The study of tracks in the olivines of the Seimchan pallasite may give new inspiring results, as well as may confirm the theoretical predictions and justify the efforts in their synthesis in the terrestrial conditions.

The work is fulfilled within the topic of GEOKHI RAS. I express my gratitude to T. A. Pavlova for the assistance in work.

References

Alexeev V.A, et al. // Short communications on physics, 2019, № 8, P. 15-22. https://ksf.lebedev.ru/contents.php?post=1&year=2019&number=08&z=0

Anders E. // Space Science Reviews. 1964.V.3. P. 583-714.

Berezinsky V.S., et al. // Astrophysics of cosmic rays. Moscow: Nauka, 1990.

Ellison D. C., Eichler D. // Astrophys. J. 1984. V. 256. P. 691-701.

Haungs A. (KASCADE –Grande Colaboration) // Highlight talk at 31-st ICRC. Lodz, 2009. http://icrc2009.uni.lodz.pl/dl.php?fname=haungs.pdf

Khisina N. R., et al. // Geochemistry International, 2020, Vol. 58, No. 9, P. 994-1003.

Markelova T.V., Snytnikov V.N. // Calculating methods and programming. 2012. V. 13. P. 443-451.

Pollack J.B. // Annual Review of Astronomy and Astrophysics. 1984. V. 22., P. 389-424.

Scott E.R.D., Taylor G.J. // The 21st LPSC. 1991. P. 1119-1120.

Tarduno, J.A., et al. // Science. 2012. V. 338. P. 939-942. (doi:10.1126/science.1223932

Ustinova G.K. // Physics of Atomic Nuclei, 2013, Vol. 76, No. 5, P. 616-655.

Ustinova G.K. // Geophysical Research Abstracts. V. 8. 00028. 2006. SRef-ID: 1607-7962/gra/EGU06-A-00028. European Geosciences Union, 2006.

Weidenschilling S.J. // Icarus. 1980., V. 44., P. 172-189.

Weidenschilling S.J., Cuzzi J.N. // Protostars and Planets III. Tucson: Univ. of Arizona Press, 1993. P. 1031-1060.